Cancer Cell(s) Cycle Sequencing Reveals Universal Mechanisms of Apoptosis

R. M. Ardito Marretta[*] **and F. Ales**[†]

Abstract: In this paper, cell cycle in higher eukaryotes and their molecular networks signals both in G_1/S and G_2/M transitions are replicated *in silico*. Biochemical kinetics, converted into a set of differential equations, and system control theory are employed to design multi-nested digital layers to simulate protein-to-protein activation and inhibition for cell cycle dynamics in the presence of damaged genomes. Sequencing and controlling the digital process of four micro-scale species networks (p53/Mdm2/DNA damage, p21mRNA/cyclin-CDK complex, CDK/CDC25/wee1/
SKP2/APC/CKI and apoptosis target genes system) not only allows the comprehension of the mechanisms of these molecule interactions but paves the way for unraveling the participants and their by-products, until now quite unclear, which have the task of carrying out (or not) cell death. Whatever the running simulations (e.g., different species signals, mutant cells and different DNA damage levels), the results of the proposed cell digital multi-layers give reason to believe in the existence of a universal apoptotic mechanism. As a consequence, we identified and selected cell check points, sizers, timers and specific target genes dynamic both for influencing mitotic process and avoiding cancer proliferation as much as for leading the cancer cell(s) to collapse into a steady stable apoptosis phase.

Keywords: cell digital biotechnology, cancer

cell cycle control, cell digital systems, protein networks signalling, apoptosis

1 Introduction

The cell cycle is a sequence of extremely complex and orderly events to vehicle into the daughters the same constituents as the mother cell (G_1, S, G_2 and M phases). In the crucial steps, G_1 and G_2, cell growth and DNA doubling take place so that the daughters have the same mass and genetic code as the parent cell. During all of the transitions, the cell passes checkpoints waiting for the "green light" for admission into the next phase. When G_2/M is accomplished, cells start a new cycle. Both in higher eukaryotes and yeast, the duty cycle period between two consecutive divisions depends on cell size which can be divided into two sub-phases, one called *sizer* and the other *timer* (see Qu et al. (2003a), Masui and Wang (1998), Montagne et al. (1999), Fantes (1977), Sveiczer et al. (1999a)).

If the initial size of the cell after the division is smaller than a critical value, *sizer* corresponds to the required time for increasing mass; meanwhile, if the size exceeds a threshold, the *timer* phase identifies the timespan of a complete division. All these cell cycle parameters are regulated and tuned by signaling protein networks arising from very complex kinases and phosphatases which are not completely understood by conventional biological methods. As a consequence, new approaches such as mathematical modeling, non linear system dynamics and digital signal analysis are increasingly employed for deeper insights into cellular biological process (see Qu et al. (2003a-b), Aguda (1999), Aguda and Tang (1999), Chen et al. (2000), Gardner et al. (1998), Golbeter (1991), Hatzimanikatis et al. (1999), Novak and

---

[*] Corresponding author. Department of Structural, Aerospace Engineering and Geotechnics, University of Palermo, Viale delle Scienze, Block 8, 90128, Palermo, (Italy). Tel. +3909123896747, Fax +39091485439. Email: romario@unipa.it

[†] Department of Aerospace Engineering and Astronautics, University of Rome, Via Eudossiana, 18, 00187, Rome, (Italy)

Tyson (1997), Obeyesekere et al., (1997); Sveiczer et al. (1999a-b), Thron (1997), Tyson et al. (2001), Tyson et al. (2002)).

Thus, increasing cooperation between biology and mathematics, due in part to the decoding of the human genome (see Ambrosi and Preziosi (2002), Ambrosi and Mollica (2002), Ambrosi and Mollica (2004), Breward et al. (2002), Byrne et al. (2003), Byrne and Preziosi (2004), Chaplain et al. (2006), Frieboes et al. (2006), Macklin and Lowengrub (2007), Panorchan et al. (2006)) and supercomputer-aided computational resources, tries to dissect the roles of cell species in coordinating several events: DNA synthesis, genome integrity check and emergence, nuclear division, cell separation, and such critical cell behaviors as repetitive cycle, checkpoints and size progression.

For these purposes, mathematical bifurcation analysis has been outstandingly successful in modeling biochemical reactors and regulators of the eukaryotes cell cycle in terms of molecular antagonisms, hysteresis, irreversible transition up to intrinsic pathway of programmed cell death (see Chen et al. (2000), Tyson et al, (2001), Tyson et al. (2002), Zhang and Henson (2001), Zhang et al. (2009), Tyson and Novak (2001)).

Nevertheless, this method shows intrinsic limitations. For example, a pure limit cycle does not exhibit cell checkpoints; meanwhile, a pure bistable system gives defined cell checkpoints but does not produce a repetitive cycle (*sic!*) (Qu et al. (2003a)). As regards cell growth, Tyson and colleagues (1998, 2001a-b, 2002) suggest an elegant saddle-node bifurcation for the G_1/S transition checkpoint and saddle-node-loop bifurcation for the G_2/M phase checkpoint, so as to return cell activities to a bistable system (where G_1 is the first stable state and S-G_2-M, the second). However, other important features, such as sizers and timers (with or without a genome aberration signal) remain to be explained.

Diametrically opposite opinions lead Qu et al. (2003a-b) to mathematically model the cell cycle using *Hopf* bifurcation analysis in which sizers and timers arise naturally as features of the cell signaling network. More rigorously, in terms

of system control theory and its mathematical implications, Zhang and Henson (2001) examined cell biochemical reactors pointwise through eigenvalue dynamics on the *Argand-Gauss* plane.

Biological systems, whether at the single cell or the organism level, certainly display elements of control that in some instances have parallels in the fields of engineering, not least the concept of feedback control. The complexity of biological networks can give rise to extremely complex behaviors, some of which are generally suppressed, whereas others are utilized for particular purposes. Hence, there is a burgeoning field of so-called (digital) systems biology that attempts to understand network complexity and control at a variety of levels. From this point of view, a multi-layered digital cell scheme offers greater convenience than alternative formalisms and/or may lead to novel biological insights that could not, at least without great difficulty, be obtained by existing approaches (see Ardito Marretta, (2009a, b), Tsourkas (2004), Deguchi, Ohashi and Sato (2005), Mooney (2006), Zhou, Chen and Zhang (2007)).

In this paper, we adopt a new strategy for modeling cell signaling networks. Based on system control theory, the proposed model architecture is quite different from those adopted until now. Cell growth protein-to-protein signaling networks and their co-factors and by-products (see Fig. 1) are firstly translated into mathematical frames and then linked to each other via multi-nested digital layers, sub-blocks and control wirings (see Figs. 2-4). This *in silico* cell master simulator makes almost obsolete the first generation of computer-aided biological cell schemes. More specifically, this cell digital layered platform becomes a powerful tool for obtaining more accurate (and much faster) characterization of cell growth parameter dynamics, including homeostasis within cell size during successive cycles, sizers and timers. The reliability and robustness of the proposed digital cell scheme are confirmed through literary evidence. Now, since the cell digital multi-layer platform allows a single dynamical mechanism on its own to take into account all features of the cell cycle digital activities—including natural or aber-

rant cell growth parameters—it is here employed to identify those species (and their mutual interactions) able to govern and control not only the transition phases $G_1/S \div G_2/M$ but also the apoptosis mechanism as an extreme defence against DNA damage proliferation.

Systems control theory is used to achieve optimal digital protein signaling control and to improve our understanding of cancer cell dynamics. In this paper, a new *next generation* digital scheme is given to greatly enhance the previously used cell master simulator (see Ardito Marretta (2009a–b)) that now includes, *in silico*, multi-layer design (see Figs. 1-5) concerning p21mRNA/cyclin-CDK complex and CDK/CDC25/wee1/SKP2/APC/CKI networks. In this model, natural and aberrant cell cycle dynamics can be easily replicated by switching different input signal pathways of p21mRNA, ionizing radiation amounts (i.e., different DNA damage levels) and timespans of action (see Figs. 2-5).

For the higher eukaryotes cell cycle under examination, once different input signal pathways of p21mRNA are injected and/or mutant species are considered, the "all-at-once" simulations of the four-based protein sub-networks complex unravel species network signaling co-factors and by-products, not yet completely understood, influencing not only the cell growth factors but, acting in synchrony within a complex digital mechanism, how they can determine (or not) the cell fate. We demonstrate that this mechanism, further discussed, is independent of cell cycle environmental input and its activation pathways line up with general principles which may thus be assumed to be universal.

2 (Biochemical) Materials and (biotechnological) methods

As previously mentioned, a nested digital multilayer has been designed *ex novo* to simulate *in silico* the cancer cell cycle by involving four interlinked micro-scale species networks: a) p53/Mdm2/DNA damage; b) p21mRNA/cyclin-CDK complex; c) CDK/CDC25/wee1/SKP2/APC/CKI, and, d) apoptosis target gene system, i.e., cyclin-dependent kinase CDK/CDC25 inhibitor, p21; p53-regulated apoptosis-inducing protein 1, p53AIP1; apoptotic protease activating factor 1, APAF1. The target gene "cytoc" is considered a functional of APAF1 in Apoptosome synthesis, expressed by the Heaviside function, equal to 1 (or zero) for matching (or not) cell death.

2.1 Biochemical assumptions and digital sublayer of p53/Mdm2/DNA network

In the cell cycle of several cancer pathologies, the oncosuppressor p53 protein induces the transcription of genes in charge of cell-cycle arrest, DNA repair and apoptosis (see Ma et al. (2005), Geva-Zatorsky et al. (2006), Shangary and Wang (2008), Ciliberto et al. (2005), Zhang et al. (2007)). The well-known Knudson model of tumorigenesis draws the conclusion that mutation of both copies of each gene of this oncosuppressor is necessary and sufficient to trigger neoplasm formation (see Knudson (1971), Fodde and Smits (2002), Hohenstein (2004)). But, other studies by Venkatachalan et al. (1998) and Song (1999) experimentally show how haploinsufficiency can violate Knudson's hypothesis, e.g., tumors can arise in mice with only one undamaged copy of the p53 transcription factor.

In the cell cycle arrest and the DNA repair actions, p53 is not a "stand-alone" actor but works in synchrony with the Mdm2 protein through ubiquitin-mediated proteolysis in such a way as to realize a biological negative feedback in which the p53 level is kept low (Ciliberto et al. (2005)). Subsequently, upon DNA damage, the ATM protein (Ataxia-Telangectasia-Mutated) kinase acts to phosphorylate the p53 to avoid binding of the Mdm2 (see Reich et al. (1983), Bates et al. (1998), Bar Or et al. (2000), Bell et al. (2002), Lahav et al. (2004), Loewer and Lahav (2006), Ventura et al. (2007), Batchelor et al. (2008)).

In a human cell, the biological response of the considered species (ATM, p53 and Mdm2) is interlinked with, and quite similar to, the output response of oscillating network dynamics, i.e., $(ATM \rightarrow p53 \rightarrow Mdm2 \mapsto |p53)$. If DNA damage exceeds a threshold, the p53 pulses to activate
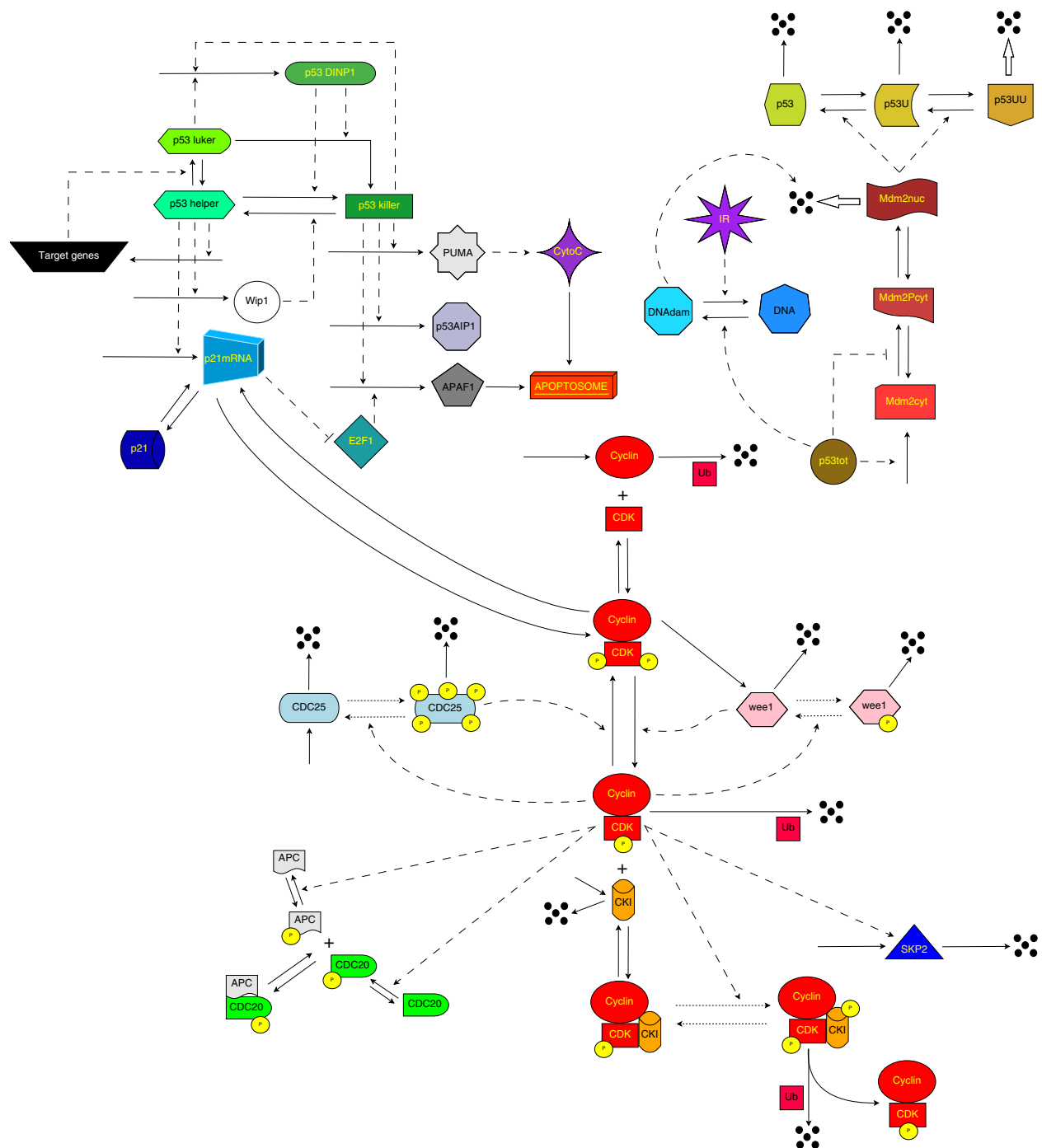
Figure 1: Wiring diagram of the molecular model of cancer cell species dynamics. Interpretation of the sketched map is that the solid lines with arrowheads represent protein synthesis or degradation or a kinase reaction step. The dashed lines indicate the protein-to-protein (connected by) catalyzation while the dotted lines represent the phosphorylation process. 5-black sphere sites represent degraded molecules. All the molecular activities are translated into a general set of differential (linear and non-linear) equations (see Tables 3-4).

transcription of the p21 gene and other species for apoptosis execution (see Ardito Marretta (2009a-b), Ghosh and Bose (2006), Bose and Ghosh (2007)).

We start by taking into account the protein forms of p53 (p53 mono-ubiquitinated, p53 poly-ubiquitinated and p53 total, i.e., $p53_U$, $p53_{UU}$ and $p53_{tot}$, respectively) and Mdm2 (nuclear, cytoplasmic and phosphorylated, i.e., $Mdm2_{nuc}$, $Mdm2_{cyt}$ and $Mdm2_{Pcyt}$, respectively) with their time-dependence upon a set of equations (Ciliberto et al. (2005)). From a biotechnological point of view, the problem consists of processing a set of ordinary differential equations (ODEs) in a computational space, the *state-space*, which mathematically represents all the possible conditions and combinations of the variables of the problem. Here, we summarize the biochemical basis upon which the p53/Mdm2/DNA damage digital sub-layer is built (Ciliberto et al. (2005)).

- Mdm2 and p53 accumulate predominantly in the nucleus.

- p53 is ubiquitin-dependent degraded in an Mdm2 catalyzed reaction.

- p53 is intended and degraded most efficiently by the proteasome when it has at least 5 ubiquitin moieties attached. We assume that the nuclear form of Mdm2 attaches only 2 ubiquitins to p53 (mono-/poly-ubiquitinated forms).

- Mdm2 transcription is induced by p53. We assume that all three forms of p53 (total, mono- and polyubiquitinated) induce Mdm2 transcription with the same level of efficiency.

- p53 transcriptional activity is considered exploited at its utmost, i.e., when 4 molecules of p53 form a tetramer.

- The cytoplasmic form of Mdm2 ($Mdm2_{cyt}$) is translocated into the nucleus when it has been phosphorylated by the AKT protein kinase.

- $Mdm2_{Pcyt}$ freely migrates into and out of the nucleus. Nuclear volume is in the range $1/10 \div 1/20$ of the cytoplasmic one.

- A long pathway governs the (indirect) opposition acting by p53 to Mdm2 nuclear entry and it involves PTEN, PIP3 and AKT according to the scheme $p53 \rightarrow PTEN \rightarrow |PIP3 \rightarrow AKT \rightarrow Mdm2_{nuc} \rightarrow |p53$. We make use of a simplified loop by taking into account that phosphorylation of $Mdm2_{cyt}$ is inhibited by $p53_{tot}$.

- In the present *in silico* simulations, a generic variable (DNA damage), DNA_{dam}, depends upon *IR* (Ionizing Radiation). We apply ionizing radiation equal to the value employed by Ciliberto et al. (2005).

- DNA_{dam} and $p53_{tot}$ activities are governed by Michaelis-Menten kinetics.

Both p53/Mdm2 positive/negative feedback loops are generated and processed via the control matrices **BB** and **K** which are located between the Mdm2 and p53 protein dynamic systems for a real-time check of the digital output variables (protein kinases and their time rates). The onset of the digital master layer is tuned to accurately replicate the results of the literature regarding irreversible and reversible DNA damage levels (see Table 5). According to the block diagram algebraic definition used, we have: an integrator block (which digitally evaluates the integral expressions, e.g., $\int x dx = x^2/2$); a "0" vector block is a zero-element vector; **BB** is a matrix block that is employed to build up the control matrix feedback, **K**, in the *LQR* (Linear Quadratic Regulator) system; the *kd2* block digitally performs the rate constant for degradation of $Mdm2_{nuc}$; the *PSD* subsystem block extracts the Power Spectral Density.

Now, biotechnological processors are applied to the continuous time-dependent p53/Mdm2 /DNA damage system (and similarly to the others) that can be summarized by:

$$\dot{\mathbf{x}} = \mathbf{A}\mathbf{x} + \mathbf{B}u \qquad (1)$$

where:

$\dot{x}$ is the derivative of the state-vector, **x**, (containing all of the variables of interest)

A is the matrix for p53 transcription factor dynamics

B is the matrix for the transition (LQR) input-state

u is the LQR input

Translation of Eq. 1 requires the introduction of a quadratic cost function defined as

$$CF = \int_0^\infty \left(x^T Q x + u^T R u \right) dt \qquad (2)$$

The feedback control law that minimizes the value of the cost function is

$$u = -Kx; \; K = R^{-1} B^T P \qquad (3)$$

where P is found by solving the continuous time algebraic Riccati equation

$$A^T P + PA - PBR^{-1} B^T P + Q = 0 \qquad (4)$$

with:

Q a semi-definite positive matrix containing, as elements, the inverse of the square maximum values of the protein concentrations

R a positive definite matrix containing, as elements, the inverse of the square maximum values of the input signals

K the control matrix feedback

P the stabilizing solution of Riccati equation (in matrix terms)

The state-vector for p53 and its concentrations is:

$$\mathbf{x(t)} \triangleq \left\{ [p53][p53_U][p53_{UU}][\dot{p53}][\dot{p53}_U][\dot{p53}_{UU}] \right\}^T \quad (5)$$

where the overdot represents the time-derivative and the subscripts U and UU identify the first- and poly-ubiquitin protein forms and T (above the right-hand square bracket) the transpose of the vector, respectively; while the vector

$$\mathbf{b} = \begin{bmatrix} k_{s53} & 0 & 0 & 0 & 0 & 0 \end{bmatrix}^T \qquad (6)$$

contains the coefficients used by Ciliberto et al. (2005). The vector **b** is defined once the state-space representation is implemented for describing the input-state relationships.

We consider the level of $[Mdm2_{nuc}(t)]$ as a time variable and a matrix **P** for the dynamic activity of p53 (time-variant). Then, Mdm2 dynamics can be expressed by a vector in the state-space. Once the proposed state-space representation gives the same results as the model of Ciliberto et al. (2005) (see also Table 5 and Ardito Marretta (2009a,b)), the digital optimal control law is implemented, based on the assumption that the matrix is such that $[Mdm2_{nuc}]$ is equal to a constant. Then, the compact expression

$$\mathbf{P} = \left\{ \underline{\underline{P_{ij}}}; i, j = 1, 2, 3 \; \text{so that } p_{ij} \in \Re \right\} \qquad (7)$$

(in which the symbols $\in$ and $\Re$ mean "belonging to" and range of real numbers, respectively), represents the time-invariant dynamic super-matrix. Using the digital scheme, the performed simulations allowed the identification of the constant value of $[Mdm2_{nuc}(t)]$ equal to 0.1 in such a way as to obtain a rate of DNA repair much more quickly than Ciliberto et al. (2005) (see also Table 5 and Ardito Marretta (2009a,b)). Once the initial conditions of stable steady-state are considered, a digital control circuit can be designed through the protein [p53] state-space representation (or the equivalent [Mdm2] in feedback), i.e.:

$$\dot{\mathbf{x}}(t) = \mathbf{P}\left([Mdm2_{nuc}(t)]\right)\mathbf{x}(t) + \mathbf{b} \qquad (8)$$

$$\mathbf{z(t)} = \left\{ [Mdm2_{nuc}][Mdm2_{cyt}][Mdm2P_{cyt}] \right. $$
$$\left. [Md\dot{m}2_{nuc}][Md\dot{m}2_{cyt}][Md\dot{m}2P_{cyt}] \right\}^T$$
$$(9)$$

$$\dot{\mathbf{z}}(t) = \dot{\mathbf{M}}\left([p53_{tot}(t)], k_{d2}(t)\right) + \mathbf{c}\left([p53_{tot}(t)]\right) \qquad (10)$$

$$\mathbf{c} = [0 \, f([p53_{tot}(t)]) \, 0 \, 0 \, 0 \, 0]^T \qquad (11)$$

where $[Mdm2_{nuc}(t)]$ defines the time-dependent oncogene concentration rate in nuclear form during the DNA repairing action. $[Mdm2_{cyt}]$ and

$[Mdm2P_{cyt}]$ are the time-dependent oncogene concentration rates in cytoplasmic and phosphorylated forms, respectively; $k_{d2}(t)$ is the rate constant for degradation of $[Mdm2_{nuc}(t)]$; the time-dependent expression $f([p53_{tot}(t)])$ represents the Hill function; meanwhile, **P** and **M** identify the dynamic matrices for the transcription factor p53 and the Mdm2 oncogene, respectively. They are obtained once a state-space representation model has been derived from the extended expression of the ODEs employed by Ciliberto et al. (2005). Mathematically speaking, the previous auxiliary matrices have been employed as follows for LQR shakedown:

$$\mathbf{K} = LQR(\mathbf{P}, \mathbf{BB}, \mathbf{Q}, \mathbf{R}) \quad (12)$$

The pre-multiplying factors of the matrices **Q** and **R** have been imposed in such a way that the pattern of the components of the state-vectors $\mathbf{x}(t)$, $\mathbf{z}(t)$ and the DNA damage are quite similar to those in the literature (Ardito Marretta, (2009a-b), Ciliberto et al. (2005)), while the optimal control matrix has to accomplish the task of accelerating the DNA repair process according to the equation:

$$\frac{d[DNA_{dam}]}{dt} =$$
$$k_{DNA}[IR] - k_{dDNA}[p53_{tot}]\frac{[DNA_{dam}]}{J_{DNA}+[DNA_{dam}]} \quad (13)$$

in which *IR* represents the functional of the imposed radiation dose; while k_{DNA}, k_{dDNA}, DNA_{dam} and J_{DNA} represent the (direct) rate constant linked to ionizing radiation, the direct constant rate linking DNA damage to the rate of transcription factor $p53_{tot}$, the amount of damaged DNA and the Michaelis constant of $p53_{tot}$-dependent DNA damage, respectively. The system of differential equations obtained must be processed and solved, i.e.:

$$\begin{cases} \mathbf{P}^T\mathbf{S} + \mathbf{SP} - (\mathbf{SBB})\mathbf{R}^{-1}(\mathbf{BB}^T) + \mathbf{Q} = \mathbf{0} \\ \mathbf{K} \equiv optimal\ control\ law\ = \mathbf{R}^{-1}(\mathbf{BB}^T\mathbf{S}) \end{cases}$$
$$(14)$$

From the first equation of the above system, one obtains the Riccati stabilizing solution **S**, and the

second equation is then solved, the optimal control matrix terms being a function of the following parameters:

$$\begin{cases} \mathbf{K} = \{k_{ij} \in \Re/\ k_{ij} \\ \quad = f(q_{ij}, r_{ij}, [Mdm2_{nuc}], k_f, k'_{d53}, k_{d53}, k_r) \\ [Mdm2_{nuc}] = const \\ q_{ij} \in \mathbf{Q} \\ r_{ij} \in \mathbf{R} \end{cases}$$
$$(15)$$

where k_f, k'_{d53}, k_{d53} and k_r are the translation rates of $[Mdm2_{nuc}]$, $[p53_{tot}]$, $[p53_{UU}]$ and the translation rate of $[p53_{UU}]$-dependent $[p53_U]$, respectively. Easy mathematical manipulation of the p53 equation yields:

$$\frac{d}{dt}[p53_{tot}] = \frac{d}{dt}[p53] + \frac{d}{dt}[p53_U] + \frac{d}{dt}[p53_{UU}]$$
$$(16)$$

and one then obtains:

$$\frac{d}{dt}[p53] =$$
$$-k_{d53'}[p53] - \left(k_{d53'}[p53_U] + \frac{d}{dt}[p53_U]\right) \quad (17)$$
$$-\left((k_{d53'}+k_{d53})[p53_{UU}] + \frac{d}{dt}[p53_{UU}]\right)$$

$$\frac{d}{dt}[p53_U] = k_f[Mdm2_{nuc}][p53]$$
$$-(k_{d53'}+k_r+k_f[Mdm2_{nuc}])[p53_U] \quad (18)$$
$$+k_r[p53_{UU}]$$

$$\frac{d}{dt}[p53_{UU}] = k_f[Mdm2_{nuc}][p53_U]$$
$$-(k_{d53'}+k_{d53}+k_r)[p53_{UU}] \quad (19)$$

Now, if the optimal control law is applied, further terms belonging to the matrix **K** must be added, and the extended form of the final system of equations is then obtained. Rearranging the system (Eq. 17, 18 and 19), one comes to:

$$\frac{d}{dt}[p53] = -(k_{d53'}+k_f[Mdm2_{nuc}])[p53]$$
$$(20)$$
$$+k_r[p53_U]+k_{s53}+\sum_{n=1}^{3}k_{1,n}x_{n,1}$$

$$\frac{d}{dt}[p53_U] = k_f [Mdm2_{nuc}][p53]$$
$$- (k_{d53'} + k_r + k_f [Mdm2_{nuc}])[p53_U]$$
$$+ k_r [p53_{UU}] + \sum_{n=1}^{3} k_{2,n} x_{n,1}$$

$$(21)$$

$$\frac{d}{dt}[p53_{UU}] = k_f [Mdm2_{nuc}][p53_U]$$
$$- (k_{d53'} + k_{d53} + k_r)[p53_{UU}] \quad (22)$$
$$+ \sum_{n=1}^{3} k_{3,n} x_{n,1}$$

Tables 1–2 show the adopted values of the matrix elements. It is worth noting the LQR employed for building up the optimal control matrix is not applied here to solve a Linear-Quadratic-Gaussian (LQG) control problem.

2.2 Biochemical assumptions and digital sub-layer of p21mRNA/cyclin-CDK complex

Working backwards, a biochemical chain kinase links p21mRNA to DNA damage (and p53/Mdm2 network) via ATM/ATR. As is commonly recognized, the p21mRNA protein inhibits the cyclin-CDK complex activity leading to a delay in the G_2/M transition or better in the cell cycle arrest. As a consequence, p21mRNA is indirectly connected to DNA damage and is capable of activating the chk1 protein which inhibits CDC25 activity. In agreement with but differently from Qu et al. (2003), Ghosh and Bose (2006), Bose and Ghosh (2007), we mathematically and digitally translate biochemical p21mRNA/cyclin-CDK chain kinase reactions into a differential equation (values of reaction constants are listed in Table 4)

$$\frac{dx}{dt} = (k_5 + f(z))x_1 \qquad (23)$$
$$- (k_6 + g(w))x - (k_7 + k_{7u}u)x - k_{14}xi + k_{15}i_x$$
$$+ (k_{16} + k_{16u}u)i_{xp} - \delta p21_{mRNA}x$$

The last term on the right-hand side proportionally connects p21mRNA to phosphorylation catalyzed by active cyclin-CDK (x) and its rate to the level of DNA damage. For digitally designing and checking the cell multi-layers, we assume

a numerical value for δ so as to obtain the same starting level of DNA damage of Qu et al. (2003).

The digital scheme of p21mRNA/cyclin-CDK complex involves a multi-nested layer. The first (see "[p21] Subsystem1" block circuitry and Sub-Block A in Fig. 3) replicates *in silico* protein-to-protein signaling among the p21 forms and all the considered species of p53 via Goldbeter-Koshland function. A digital switching chain (see Sub-Block B of Fig. 3) injects several combinations of p21mRNA input signal during cell cycle transition phases. Here, two species of p21 are considered, i.e., p21 inactive and p21mRNA; only p21mRNA is considered in feedback with active cyclin-CDK complex.

2.3 Biochemical assumptions and digital sub-layer of CDK/CDC25/wee1/SKP2-/APC/CKI network

Following Qu et al. (2003a-b) and the proteins kinase map of Figure 1, the biochemical synthesis of the considered species has been translated into differential equations (see Tables 3 and 4).

Cyclin-CDK (together with cyclin A, B and E) are the most important cyclin-dependent kinases in higher eukaryotes and they mark (with two different expressions, inactive and active) both G_1/S and G_2/M phases. In any case, both expressions can be modeled by the current digital model for the cell cycle transitions. Inactive cyclin-CDK is obtained by phosphorylating CDK at Thr14 and Tyr15 which are, at the same time, dephosphorylated by CDC25. Thus, wee1 acts to restore the phosphorylation process at Thr14 and Tyr15, inactivating this kinase activity. Digitally speaking, CDC25 must be phosphorylated by active cyclin-CDK complex for becoming active and giving a positive feedback loop. Conversely, wee1 becomes inactive via its phosphorylation which is catalyzed by active cyclin-CDK complex so giving a double-negative feedback loop (equivalent to a single positive feedback loop). In sequence, active cyclin-CDK is inhibited via its inhibitor, CKI. In turn, CKI bound to cyclin-CDK is degradable after being phosphorylated by active cyclin-CDK. This degradation again frees cyclin-CDK and another positive digital loop can be modeled
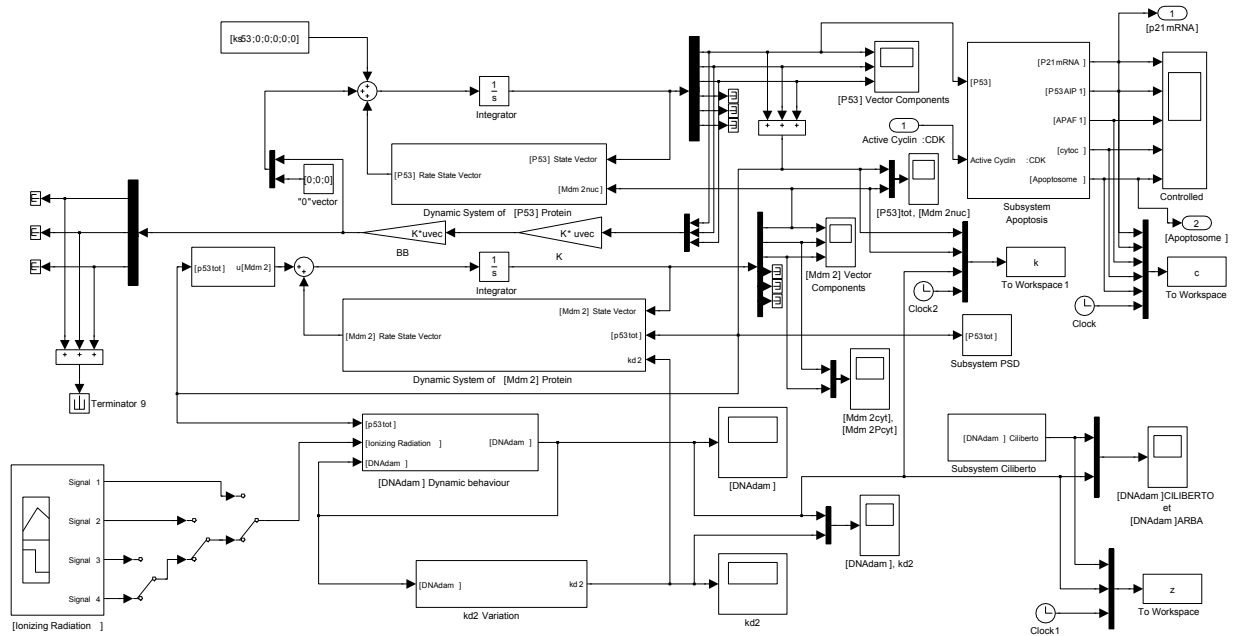
Figure 2: Human cell DNA damage-repair master digital simulator (overall view): the main blocks calculate the p53/Mdm2/DNA network dynamics once the input signal of ionizing radiation is processed by a devoted sub-block; both p53/Mdm2 positive/negative feedback loops are generated and digitally processed. The control matrices (**BB** and **K**) are located between the Mdm2 and p53 protein dynamic systems for a real time check of the digital output variables (see §*2.1* for components details).

(see also Table 3 for the representative ODEs). CDC25 plays a fundamental role in cell dynamics because its phosphorylation sites are phosphorylated during two cell cycle transitions. Without loss of generality, we assume that CDC25 has two phosphorylation sites and is constantly synthesized at a rate, k_8. In the protein map of Figure 1, all the CDC25 forms are degraded via their concentration-dependent constant, k_9 (for the values of these constants see Table 4) (see Vlach et al. (1997), Montagnoli et al. (1999), Fotedar et al. (2008), Dealy et al. (1999), Wang et al. (1999), Morris et al. (2000), Nakayama et al. (2001)). As regards wee1, its role was partially examined within phosphorylation restoring action at Thr14 and Tyr15 and its inactivity caused by active cyclin-CDK complex. Following Qu et al. (2003a-b), we suppose a constantly synthesized wee1 (rate equal to k_{10}) its unphosphorylated and phosphorylated forms being proportionally degraded with their expressions. As a consequence, only the unphosphorylated wee1 is active in this

process. Similarly to other considered species, SKP2 degradation follows a linear (proportional) ramp with concentration, i.e., dSKP2/dt=αh(x)-βSKP2, where αh(x) and β identify the activation rate of SKP2, via active cyclin-CDK(x) and the inaction rate of SKP2, respectively. APC becomes active through a double-process, i.e., it has to be phosphorylated and then bind to the phosphorylated form of CDC20. The loop is closed in chain by active CDK1 which directly and indirectly catalyzes both APC and CDC20. Similarly to SKP2, we assume again $dAPC/dt = \alpha h(x) - \beta APC$ (see also Table 4 for the obtained differential equations). The cyclin-CDK-CKI complex is phosphorylated by active cyclin-CDK for its degradation (see Vlach et al., 1997, Montagnoli et al., 1999). Proportionally to its concentration, degradation of CKI occurs with synthesis constant rate k_{12}. SCF and SKP2 facilitate the degradation of phosphorylated CKI complexed with cyclin-CDK through differential equation in Table 4. Quite similar to an advanced computer-based
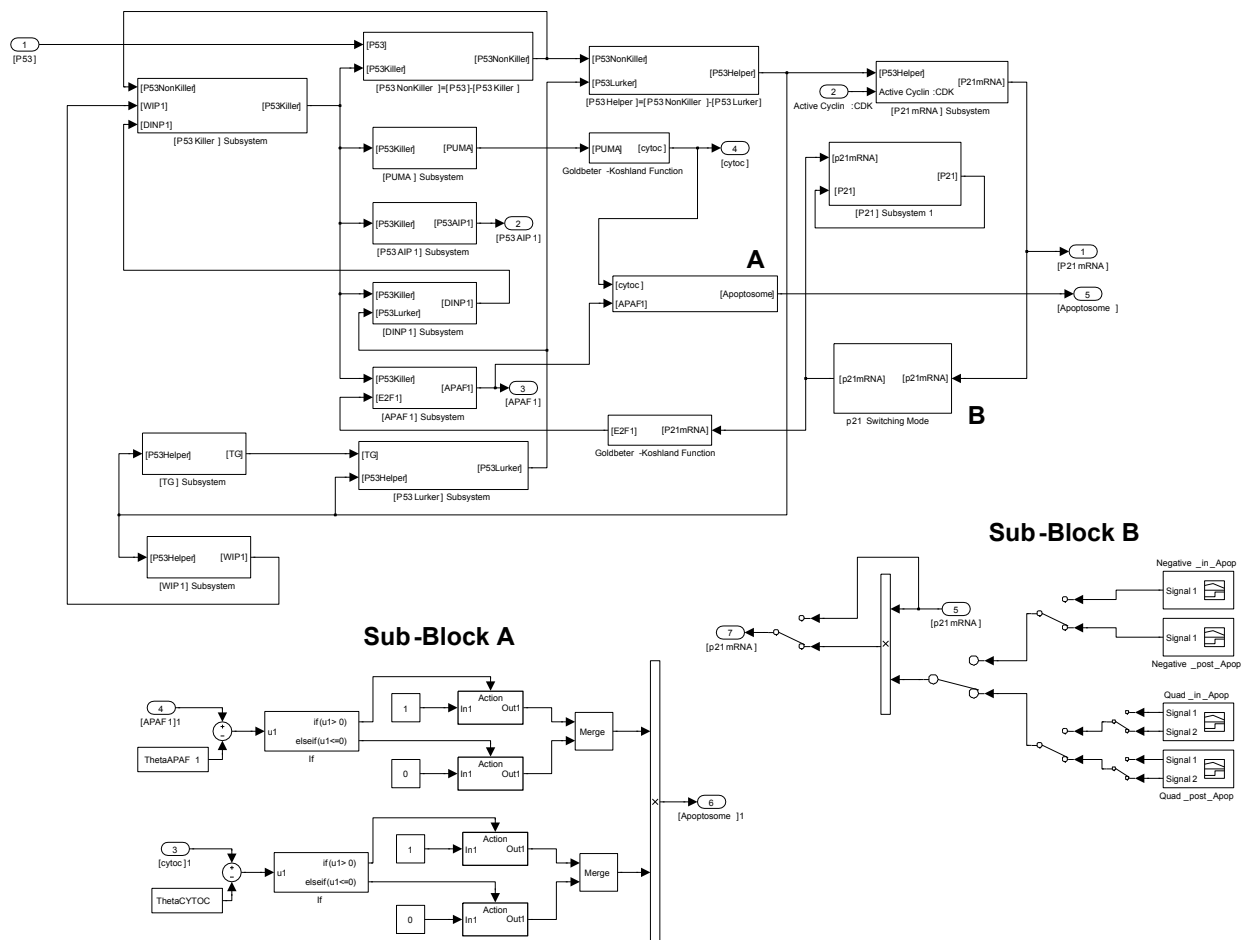
Figure 3: Digital sub-networks of p21mRNA/p21 and apoptotic target genes (p53$_{killer}$, p53$_{helper}$, p53$_{lurker}$, p53AIP1, PUMA, DINP1, WIP1, E2F1, APAF1, cytoc and Apoptosome). **Sub-block A**: apoptosis network control layer. If $p53_{helper}$-induced phosphatase Wip1 exceeds $p53_{lurker}$-induced kinase p53DINP1, then p53 signals consist of "helpers" and "lurkers". As Wip1 decreases while p53DINP1 increases, via transformation of $p53_{helper}$ into $p53_{lurker}$, $p53_{killer}$ begins to accumulate (Wip1 and $p53_{killer}$ subsystems). If DNA damage is quickly repaired, PUMA, p53AIP1, p53DINP1 and APAF1 subsystems are not activated. On severe DNA damage, the apoptosis network starts to pulse for accumulation of $p53_{killer}$, PUMA-cytoc and $p53_{helper}$; Apoptosome and p21mRNA subsystems are designed to match a steady-stable apoptosis phase. **Sub-block B**: p21mRNA input signal switching layer. We suppose the p21mRNA has different signal pathways over different triggering timespans: the signaling outfits of p21mRNA are distinct mono-cycle square-waves enclosed within three different timespans of [0÷200min], [114.4÷144.85min (natural apoptotic time window, see Ardito Marretta 2009a-b)] and [200÷1200min], respectively; afterwards, we change the mono-cycle square-wave into a negative linear-ramp signal acting in the last two assigned timespans. (see also Ardito Marretta 2009a-b)

Figure 4: Cell cycle master digital simulator: the main blocks ("*Cell Division Control System*", "*Cell Cycle Dynamics*", "*Cell sizer & check point control system*") simulate the cell sizer, timer and checkpoint network dynamics once the simulation is processed; all key role cell division species (APC, SKP2, cyclin-CDK, CDC25, wee1, CKI) positive/negative feedback loops are designed and digitally processed. Oscillatory scopes are added for monitoring the involved pulsing species over the assigned timespans. **Sub-block A**: Cell division control system. In this layer, in agreement with experimental evidence and specific literature, the APC/cyclin-CDK-dependent cell division signals are triggered and processed within the "*Cell sizer & check point control system*". **Sub-block B**: *State-space* of the cyclin-CDK. Through a vector representation in the state-space of the mutual interaction among free cyclin, inactive cyclin-CDK complex, active cyclin-CDK complex, total CDK and free CDK, a control digital layer acting in positive (or negative) feedback is obtained and processed.

Figure 5: Digital sub-network of cell cycle activities (clockwise: division, cell fate, growth and growth arrest): the macro-block containing sub-blocks A and B runs to simulate the cell division process. Its digital scheme faithfully reproduces the experimental evidence of cell proliferation (see Table 5 and Qu et al. (2003a)); once the involved species (APC and active cyclin-CDK) concentration dynamics reaches a threshold value, the "Cell Division ControlSystem" (see Fig. 4) processes and pings a control signal towards sub-block A and "Switch 1"; these digital elements promote division phase within cell cycle. **Sub-Block A**: Stand-alone cell growth digital simulation layer. This sub-block captures the key dynamical features of cell duplication mathematically described (see Table 3) in which checkpoints, sizers and timers are respectively governed by the current DNA damage level, cell mass growth and species expression. **Sub-Block B**: Apoptosis control layer. Cell mass is directly controlled from G_1/S to G_2/M transitions by the apoptotic target gene network; cell death is matched and becomes steady stable if Apoptosome = 1 all over the timespan.

Table 1: **Parameters for the p53/Mdm2 network model**

Parameters	Description	Values
f	Hill function	
$q_{ij} \in \underline{\underline{Q}}$	Bryson rule matrix diagonal elements (*LQR*)	$1min^{-1}$
$r_{ij} \in \underline{\underline{R}}$	Bryson rule matrix diagonal elements (*LQR*)	$0.5min^{-1}$
k_{s53}	Rate of overexpressed $p53_{tot}$	$0.055min^{-1}$
k_{d53}	Rate of $p53_{UU}$ degradation	$8min^{-1}$
k'_{d53}	Rate of $p53_{tot}$ degradation	$0.0055min^{-1}$
k_f	Rate of $Mdm2_{nuc}$-dependent $p53_U$ degradation	$8.8min^{-1}$
k_r	Translation rate of $p53_{UU}$	$2.5min^{-1}$
k_{DNA}	Rate IR-dependent DNA damage	$0.18min^{-1}$
k_{dDNA}	Rate of $p53_{tot}$ degradation-dependent DNA damage	$0.017min^{-1}$
IR	Ionizing Radiation	
J_{DNA}	State variable in Hill function for DNA repair	1
ampl	IR dose amplitude unit	1

Table 2: **Optimal control matrix coefficients**

Matrix elements	Description	Constant
k_{11}	Digital optimal control matrix element	$0.0023min^{-1}$
$k_{12}=k_{21}$	Digital optimal control matrix element	$0.0017min^{-1}$
$k_{13}=k_{31}$	Digital optimal control matrix element	$0.0004min^{-1}$
k_{22}	Digital optimal control matrix element	$0.0015min^{-1}$
$k_{23}=k_{32}$	Digital optimal control matrix element	$0.0004min^{-1}$
k_{33}	Digital optimal control matrix element	$0.0001min^{-1}$

Table 3: Mathematical model

Governing equations	Notes

$\frac{dp53_{tot}}{dt} = k_{s53} - k_{d53'}p53_{tot} - k_{d53}p53_{UU}$

$\frac{dp53_U}{dt} = k_f Mdm2_{nuc}p53 + k_r p53_{UU} - p53_U\left(k_r + k_f Mdm2_{nuc}\right) - k_{d53'} \cdot p53_U$

$\frac{dp53_{UU}}{dt} = k_f Mdm2_{nuc}p53_U - p53_{UU}k_r - p53_{UU}\left(k_{d53'} + k_{d53}\right)$

$\frac{dMdm2_{nuc}}{dt} = V_{ratio}\left(k_i Mdm2_{Pcyt} - k_0 Mdm2_{nuc}\right) - k_{d2}Mdm2_{nuc}$

$\frac{dMdm2_{cyt}}{dt} = k_{s2'} + \frac{k_{s2}p53_{tot}^m}{J_S^m + p53_{tot}^m} - k_{d2'}Mdm2_{cyt} + k_{deph}Mdm2_{Pcyt} - \frac{k_{ph}}{J_{ph} + p53_{tot}}Mdm2_{cyt}$

$\frac{dMdm2_{Pcyt}}{dt} = \frac{k_{ph}}{J_{ph} + p53_{tot}}Mdm2_{cyt} - k_{deph}Mdm2_{Pcyt} - k_i Mdm2_{Pcyt} + k_0 Mdm2_{nuc} - k_{d2}'Mdm2_{Pcyt}$

Continued on next page

Table 3 – continued from previous page

$$\frac{dDNA_{dam}}{dt} = k_{DNA}IR - k_{DNA}p53_{tot}\frac{DNA_{dam}}{J_{DNA}+DNA_{dam}}$$

$$k_{d2} = k'_{d2} + \frac{DNA_{dam}}{J_{DNA}+DNA_{dam}}k''_{d2}$$

$$p53 = p53_{tot} - (p53_U + p53_{UU})$$

$$Mdm2_{tot} = Mdm2_{cyt} + \frac{1}{V_{ratio}}Mdm2_{nuc} + Mdm2_{Pcyt}$$

$$IR = \text{ionizing radiation dose } (t=10) \tag{1}$$

$$\frac{dp53_{killer}}{dt} = DINP1\frac{p53_{nonkiller}}{0.1+p53_{nonkiller}} - Wip1\frac{p53_{killer}}{0.1+p53_{killer}}$$

$$p53_{nonkiller} = p53 - p53_{killer}$$

$$\frac{dp53_{lurker}}{dt} = k_{TG}p53 TG\frac{p53_{helper}}{0.1+p53_{helper}} - \theta_{TG}\frac{p53_{lurker}}{0.1+p53_{lurker}}$$

$$p53_{helper} = p53_{nonkiller} - p53_{lurker}$$

$$\frac{dTG}{dt} = k'_{sTG} + k''_{sTG}\frac{p53_{helper}^3}{J_{sTG}^3+p53_{helper}^3} - k_{dTG}TG$$

$$\frac{dWip_1}{dt} = k'_{sWip1} + k''_{sWip1}\frac{p53_{helper}^3}{J_{sWip1}^3+p53_{helper}^3} - k_{dWip1}Wip1$$

$$\frac{dp21}{dt} = k'_{sp21} + k''_{sp21}\frac{p53_{helper}^3}{J_{sp21}^3+p53_{helper}^3} - k_{dp21}p21$$

$$\frac{dDINP1}{dt} = k'_{sDINP1} + k''_{sDINP1}\frac{p53_{lurker}^3}{J_{sDINP1lurker}^3+p53_{lurker}^3} + k'''_{sDINP1}\frac{p53_{killer}^3}{J_{sDINP1killer}^3+p53_{killer}^3} - k_{dDINP1}DINP1$$

$$\frac{dPUMA}{dt} = k'_{sPUMA} + k''_{sPUMA}\frac{p53_{killer}^3}{J_{sPUMA}^3+p53_{killer}^3} - k_{dPUMA}PUMA$$

$$\frac{dp53AIP1}{dt} = k'_{sp53AIP1} + k''_{sp53AIP1}\frac{p53_{killer}^3}{J_{sp53AIP1}^3+p53_{killer}^3} - k_{dp53AIP1}p53AIP1$$

$$\frac{dpAPAF1}{dt} = k'_{sAPAF1} + k''_{sAPAF1}\frac{p53_{killer}^3}{J_{p53killer}^3+p53_{killer}^3}\frac{E2F1^3}{J_{E2F1}^3+E2F1^3} - k_{dAPAF1}APAF1$$

$$E2F1 = G(\theta_{p21}, p21, 0.1, 0.1) \tag{2}$$

$$cytoc = G(PUMA, \theta_{PUMA}, 0.1, 0.1) \tag{2}$$

Table 3 – continued from previous page

$$Apoptosome = H\left(APAF1 - \theta_{APAF1}\right) * H\left(cytoc - \theta_{cytoc}\right) \tag{3}$$

$$\frac{dp21_{mRNA}}{dt} = j_{21}\frac{k_a''}{k_a'' + k_d} - \gamma_m p21_{mRNA} - \delta p21_{mRNA}x$$

$$\frac{dp21}{dt} = j_{p21}p21_{mRNA} - \gamma_{p21}p21$$

$$k_a'' = k_a\frac{\left[\frac{p53_{helper}}{k_{21}}\right]^4}{1 + \left[\frac{pa}{k_{21}}\right]^4}$$

$$\frac{dy}{dt} = k_1 + k_4 x_1 - k_3 yc - (k_2 + k_{2u}u)y$$

$$\frac{dx_1}{dt} = k_3 yc + (k_6 + g(w))x - k_4 x_1 - (k_5 + f(z))x_1 \tag{4}$$

$$\frac{dx}{dt} = (k_5 + f(z))x_1 - (k_6 + g(w))x - (k_7 + k_{7u}u)x - k_{14}xi + k_{15}i_x + (k_{16} + k_{16u}u)i_{xp} - \delta p21_{mRNA}x \tag{4}$$

$$\frac{dz_0}{dt} = k_8 + k_z^- z_1 - k_z^+ z_0 - k_9 z_0 \tag{2}$$

$$\frac{dz_1}{dt} = k_z^+ z_0 + k_z^- z_2 - k_z^- z_1 - k_z^+ z_1 - k_9 z_1 \tag{5}$$

$$\frac{dz_2}{dt} = k_z^+ z_1 - k_z^- z_2 - k_9 z_2 \tag{5}$$

$$\frac{dw_0}{dt} = k_{10} + k_w^- w_1 - k_w^+ w_0 - k_{11}w_0 \tag{6}$$

$$\frac{dw_1}{dt} = k_w^+ w_0 - k_w^- w_1 - k_{11}w_1 \tag{6}$$

$$\frac{du}{dt} = \frac{(h(x) - u)}{\tau}$$

$$h(x) = \frac{x^2}{x^2 + a^2}$$

$$\frac{di}{dt} = k_{12} - k_{13}i - k_{14}xi + k_{15}i_x$$

$$\frac{di_x}{dt} = k_{14}xi - k_{15}i_x + k_i^- i_{xp} - k_i^+ i_x \tag{7}$$

$$\frac{di_{xp}}{dt} = k_i^+ i_x - k_i^- i_{xp} - (k_{16} + k_{16u}u)i_{xp} \tag{7}$$

$$s(t) = s_0 e^{\mu t}$$

$$k_1 = \frac{\kappa s(t)}{[s_c + s(t)]}$$

Continued on next page

Table 3 – continued from previous page

(1) Ionizing radiation amplitude = 1

(2) Goldbeter-Koshland function $(G(u,v,q,r))$ defined as $G(u,v,q,r) = \dfrac{2ur}{v-u+vq+ur+\sqrt{(v-u+vq+ur)^2-4ur(v-u)}}$

(3) Heaviside function $(H(x))$ defined as $H(x) = \begin{cases} 1 \text{ if } x > 0 \\ 0 \text{ if } x < 0 \end{cases}$

(4) In this model, we assign $f(z) = z_2$ since previous studies showed that two-site phosphorylated CDC25 was necessary for the occurrence of interesting dynamics. Since wee1 is inactivated after phosphorylation, we assign $g(w) = w_0$.

(5) $k_z^+ = b_z + c_z x$ is the rate constant for CDC25 phosphorylation while $k_z^- = a_z$ is for dephosphorylation.

(6) $k_w^+ = b_w + c_w x$ is the rate constant for wee1 phosphorylation while $k_w^- = a_w$ is for dephosphorylation.

(7) $k_i^+ = b_i + c_i x$ is the rate constant for CKI phosphorylation while $k_i^- = a_i$ is for dephosphorylation.

Table 4: Parameters for the 4 micro-networks-based cell layers

Rate constants	Dimensions
$k'_{s2} = 0.0015$ $k_{s2} = 0.006$ $k'_{d2} = 0.01$ $k''_{d2} = 0.01$ $k_{ph} = 0.05$ $k_{deph} = 6$ $k_i = 14$ $k_0 = 0.5$	(min^{-1})
$k_{s53} = 0.055$ $k_{d53} = 8$ $k'_{d53} = 0.0055$ $k_f = 8.8$ $k_r = 2.5$ $k_{DNA} = 0.18$ $k_{dDNA} = 0.017$ $k_{TGp53} = 3$	(")
$\theta_{TG} = 1.5$ $k'_{sTG} = 0.004$ $k''_{sTG} = 0.5$ $J_{sTG} = 1.7$ $k''_{dTG} = 0.01$ $k'_{sWip1} = 0.02$ $k''_{sWip1} = 1.2$ $J_{sWip1} = 1.8$	(")
$k_{dWip1} = 0.2$ $k'_{sp21} = 0.004$ $k''_{sp21} = 5$ $J_{sp21} = 2$ $k'_{sDINP1} = 0.004$ $k''_{sDINP1} = 0.5$ $J_{sDINP1lurker} = 0.7$	(")
$k'''_{sDINP1} = 1$ $J_{sDINP1killer} = 0.5$ $k'_{sPUMA} = 0.04$ $k''_{sPUMA} = 1$ $J_{sPUMA} = 0.3$ $J_{E2F1} = 0.3$	(")
$k_{dPUMA} = 0.5$ $k'_{sp63AIP1} = 0.04$ $k''_{sp63AIP1} = 1$ $J_{sp63AIP1} = 0.3$ $k_{dp63AIP1} = 0.5$ $k'_{sAPAF1} = 0.04$	(")
$k''_{sAPAF1} = 2$ $J_{p53killer} = 0.3$ $k'_{dAPAF1} = 0.5$ $\theta_{PUMA} = 0.5$ $\theta_{APAF1} = 0.5$ $\theta_{cytoc} = 0.5$	(")
$k'_{TGp53} = 3$ $\theta_{TG} = 1.5$ $k'_{sTG} = 0.004$ $k''_{sTG} = 0.5$	(")

Table 4 – continued from previous page

$j_{21} = 0.4\ k_d = 10\ \gamma_m = 0.01\ j_{p21} = 2\ \gamma_{p21} = 0.005\ k_a = 10\ k_m = 2\ k_{p21} = 1$ (")

Dimensionless rate constants

$m = 3\ J_s = 1.2\ J_{dam} = 0.2\ J = 0.1\ V_{ratio} = 15\ J_{DNA} = 1$

$k_1 = 300\ k_2 = 5\ k_3 = 30\ k_4 = 30\ k_5 = 0.1\ k_6 = 1\ k_7 = 10\ k_8 = 100$

$k_9 = 1\ k_{10} = 10\ k_{11} = 1\ k_{12} = 0\ k_{13} = 1\ k_{14} = 1\ k_{15} = 1\ k_{16} = 2$

$k_{2u} = 50\ k_{7u} = 0\ k_{16u} = 25\ c_0 = 200\ a = 4\ \tau = 4\ a_z = 10\ a_w = 10$

$a_i = 10\ b_z = 0.1\ b_w = 0.1\ b_i = 0.1\ c_z = 1\ c_w = 1\ c_i = 1\ s_0 = 6$

$\mu = 5.8 \times 10^{-4}\ \kappa = 479.17\ s_c = 19.93\ \delta = 0.036$

Table 5: Reliability check of the digital model

targets	timespan (min)					comments (experimental results)
	0	300	600	900	1200	
$p53$	0.1	0.0239	0.331	0.0385	0.075	Ciliberto et al. (2005)
$Mdm2_{nuc}$	0.33	0.983	0.093	0.58	0.31	(")
DNA_{dam}	0	0.408	0.30	0.029	0.021	(")
$IR\ [Gy]$	1	0	0	0	0	(")
	0	50	100	150	200	
$p53_{helper}$	0.075	0.075	0	0	0.025	Zhang et al. (2007)
$p53_{killer}$	0	0	1.54	0.112	0.1	(")

Table 5 – continued from previous page

$p53_{lurker}$	0.105	0.105	0	0	0	(")
DNA_{dam}	0	6	2	0	0	(")

	frequency (timers) [Hz]	peak (sizers)	
active cyclin − CDK	4.3×10^{-3}	18.97	Qu et al. (2003a)
Cell mass	4.3×10^{-3}	12	(")

architecture, the digital sub-layers of Figures 4 and 5 represent the central processing unit of the overall cell digital master simulator. This unit performs the biotechnological task of processing the obtained digital signals of the cell cycle (dynamical) division species (APC, SKP2, cyclin-CDK, CDC25, wee1, CKI) in positive/negative feedback loops and gives orders to Sub-Blocks A and B (see Fig. 4) of sequencing and controlling cell checkpoints, timers and sizers for all the input variables of the considered four micro-scale species networks previously mentioned. Cell cycle transitions are processed by sub-layers of Sub-Blocks (see Fig. 5) and interlinked to cell growth and division dynamics, growth arrest and cell fate. According to the proposed digital architecture and control theory, DNA damage network, cell apoptosis and cell growth arrest wirings networks (see blue, orange and green blocks of Fig. 5) can be disconnected if cell growth arrest is not considered (see more functional details in the captions of Figs 4 and 5).

2.4 Biochemical assumptions and digital sub-layer of apoptosis: APAF1, (p53)DINP1, (p53)AIP1, cytoc and Apoptosome species network

As regards the molecular kinetics for apoptosis network (see Fig. 1), we consider that $p53_{killer}$ activates PUMA, p53DINP1 and p53AIP1 genes. On the other hand, PUMA induces release cytoc to activate—in cascade—APAF1 and caspase9. The APAF1 binds both p53 and E2F1; these last two molecules play a key role in efficiently producing APAF1. It is assumed that the p53 phosphorylation on Ser46 depends on the amount of p53DINP1 and Wip1; if p53DINP1 is overexpressed (when compared to Wip1), Ser46-dependent phosphorylation of p53 gives the $p53_{killer}$ form. The roles of $p53_{helper}$ are summarized as follows: $p53_{helper}$ preferentially induces p21mRNA which in turn induces cell cycle arrest and gives time for DNA damage repair; arresting CDK activity, p21mRNA indirectly produces the retino-blastoma protein binding and inhibiting E2F1, thereby arresting APAF1 production; $p53_{helper}$ blocks backwards $p53_{killer}$ by

activating Wip1 which inhibits Ser46 phosphorylation. The last form of p53, i.e, $p53_{lurker}$ can be turned into $p53_{killer}$ by p53DINP1. p53, $p53_U$ (monoubiquitinated) and $p53_{UU}$ (polyubiquitinated) refer respectively to 0, 1 and 2 moieties attached and their sum represents the total p53 ($p53_{tot}$).

In this model, while the cytochrome C is released (Apoptosome), it binds to the cytosolic protein APAF1 and the Caspase8-dependent cytoc is activated; the wild-type of p53 (p53AIP1) is tetra-dependent both on E2F1 (inhibited by p21) and on three forms of p53 wild-type ($p53_{killer}$, $p53_{lurker}$ and $p53_{helper}$). The resulting kinase scheme - experimentally confirmed by Zhang et al. (2007) and digitally translated - displays the pathways of species according to:

$$p53_{helper}p53_{killer} \rightarrow p53AIP1 \rightarrow cytoc \\ \rightarrow Apoptosome \tag{24}$$

$$p21mRNA - |E2F1 \rightarrow APAF1 \\ \rightarrow Apoptosome \tag{25}$$

$$p53_{helper}p53_{lurker} \rightarrow p53DINP1 \tag{26}$$

$$Wip1 + p53DINP1 \rightarrow [p53_{helper}p53_{killer}] \tag{27}$$
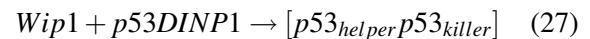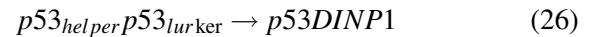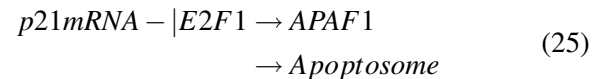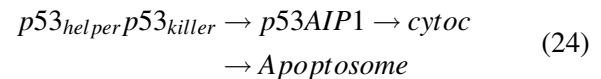
the third kinase being in back-reaction. The apoptotic species scheme is built up by multi-nested layers: by-wire connections interlink "*Subsystem Apoptosis*" diagram (see Fig. 2) to p53 forms and cyclin-CDK sub-blocks; also the p21mRNA digital block (see Fig. 3) and the sub-layers of "*Cell Division Control System*", "*Cell Cycle Dynamics*" and "*Cell sizers & checkpoint control system*" (see Figs 4 and 5) trigger concurrent and dialoguing signaling with apoptosis target genes network.

2.5 Cell cycle arrest on DNA damage target genes response

At first, the digital kinase master simulator was employed to physiologically simulate a complete cell cycle response to DNA damage including growth factors and transition dynamical processes. Separately, two square-wave radiation signals were emitted to cause a fixed level of DNA damage and evaluate (if any) sizer, timer and

checkpoint variations. The onset of these two distinct signals is tuned and imposed for 10min both in the G_1 phase (at t=50min) and in G_2/M transition phase (at t=1100min), respectively.

Plots of apoptotic target gene responses to DNA damage impulse at t=50min (see Fig. 6) reveal double-pulsing features of p21mRNA along the timespan (Fig. 6 above). In more detail, after a quiescent state, within 200÷250min, p21mRNA starts to raise its level of synthesis according to a first instability in the p53AIP1, APAF1 and cytoc pathways; looping in chain, for this time window, p21mRNA underexpression runs chorally with a low speed degradation rate of APAF1.

Once a second instability of the apoptotic species occurs, 250÷300min, p21mRNA radically changes its pathway and increases with high speed synthesis rate. Inside the range 250<t<2000min, p21mRNA oscillation pulses with a constant amplitude and lower frequency. For the time window 2000<t<5000min (digitally, t→∞), p21mRNA expression enters stable, undamped oscillation and begins to pulse in-phase with active cyclin-CDK frequency (see also Fig. 7). Conversely, the APAF1 degradation (inverse) gradient increases and its concentration falls during the timespan 200÷300min; past this time window, it remains quiescent.

This novel molecular digital multi-layer processor compensates for the discrepancy in the bifurcation analysis models (saddle-node-loop and *Hopf* bifurcations) with faster processing speed and better accuracy in the light of experimental evidence. For example, the digital p21mRNA dynamics confirms the bifurcation analysis of the cyclin-CDK complex carried out by Qu et al. (2003a) and fits quite well the results of those authors (see Fig. 7 and Table 5). The digital simulations make the mutual dynamics of these two species, active cyclin-CDK and p21mRNA, regulated with a negative feedback loop (see Fotedar et al. (2008)) almost superimposable with those obtained by bifurcation analysis (see Qu et al., 2003a) and confirm the p21mRNA low speed synthesis rate. Instead, cell species signaling networks involve high speed rate of p21mRNA synthesis as a response to the damaged genome (see Zhang et

al. (2007), Bose and Ghosh (2007)). Comparisons between cell growth regulation species (see Fig. 7) with undamaged cell cycle (see Qu et al. (2003a)), show delay in active cyclin-CDK (as well as APC) synthesis causing a variation in the "natural" cell cycle timespan. This cell cycle time window delay is equal to the cell growth time window arrest. Looking at the cell mass and active wee1 dynamics panels (Fig. 7), after a transient regarding the first two instabilities of p53AIP1, APAF1, cytoc and the first two oscillations of p21mRNA, one has to note that these cell parameters pulse in-phase with APC and active cyclin-CDK complex. Thus, only the cellular timer phase is affected by DNA damage repair while checkpoints and sizers remain steady stable.In the second simulation (see Fig. 8), DNA damage triggers at t=1100min and cell network species show absence of a bistable behavior of active cyclin-CDK in mitotic phase (see Qu et al. (2003)); this implies no modifications in p21mRNA response to DNA damage repair. Within the timespan 1150÷1950min, the cell begins dividing into two daughter cells and the increasing cyclin-CDK complex activity acts to inhibit p21mRNA overexpression in the mother cell. APC, cell mass and wee1 panels (see Fig. 9) pictorially display the ability of cell digital multi-layer platforms to describe cell checkpoints, timers and sizers. Here, differently from the previous simulation (DNA damage at t=50min), the cell cycle steps forward the time window 1150÷1950min in which G_2/M transition occurs and differences between the two performed simulations become more evident. Strictly speaking, at G_2/M, high speed activities of cyclin-CDK complex are combined with the p21mRNA modified pulsing pathway (lowest peak and highest frequency); when the mitotic process (*M* phase) is accomplished, p21mRNA decreases its frequency (and highest peak of concentration) in the daughter cells and re-enters a steady state undamped oscillation in phase with active cyclin-CDK complex, APC and wee1. As a consequence, the cell growth time arrest is equal to the delay of cell cycle species synthesis and cell checkpoint, timer and sizer behaviors are the same as those evaluated at t=50min.
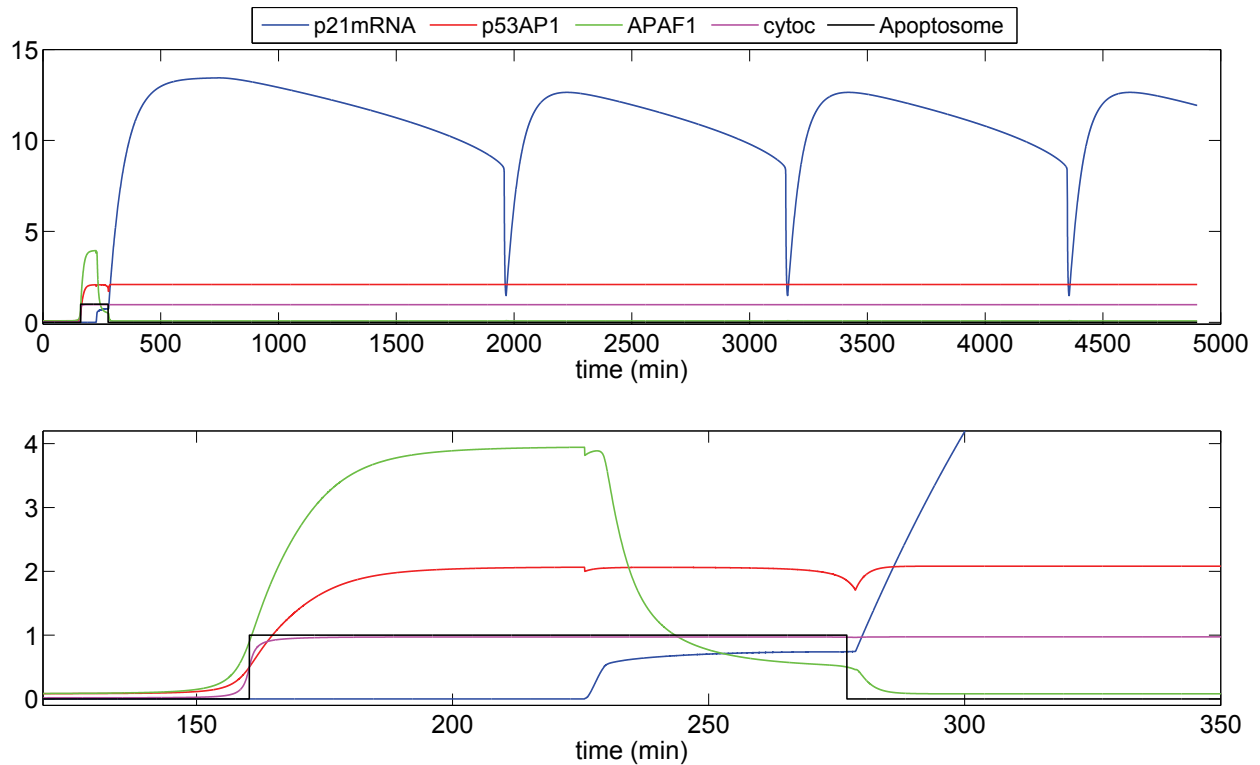
Figure 6: Output response of apoptotic species network as a consequence of DNA damage at $t = 50min$: pictorially, the species digital pathways simulate growth arrest until DNA damage level is completely repaired (see cell mass panel of Fig. 7). p21 (and Wip1, not displayed) are expressed earlier than p53DINP1 according to the experimentally observed facts (see Fiscella et al. 1997 and Oda et al. 2000). Apoptosome triggers to a digital value equal to 1 when the apoptosis phase starts. This occurs when the other target genes invert their time rates all at once, p21mRNA being almost quiescent over the complete apoptotic timespan. p21mRNA overexpression triggers at the lowest time rates of the target genes. Specifically, p53APAF1 is induced by E2F1 (degraded by p21) and $p53_{killer}$; p53AIP1 is activated by p53DINp1 via $p53_{killer}$ and $p53_{lurker}$; the cytoc gene depends on PUMA via the $p53_{lurker}$-$p53_{helper}$ back reaction. The considered timespan of 0÷5000min is adopted for obtaining stable division cell cycles (above). A close-up of the apoptosis time window is shown within the timespan 120÷350min (below).
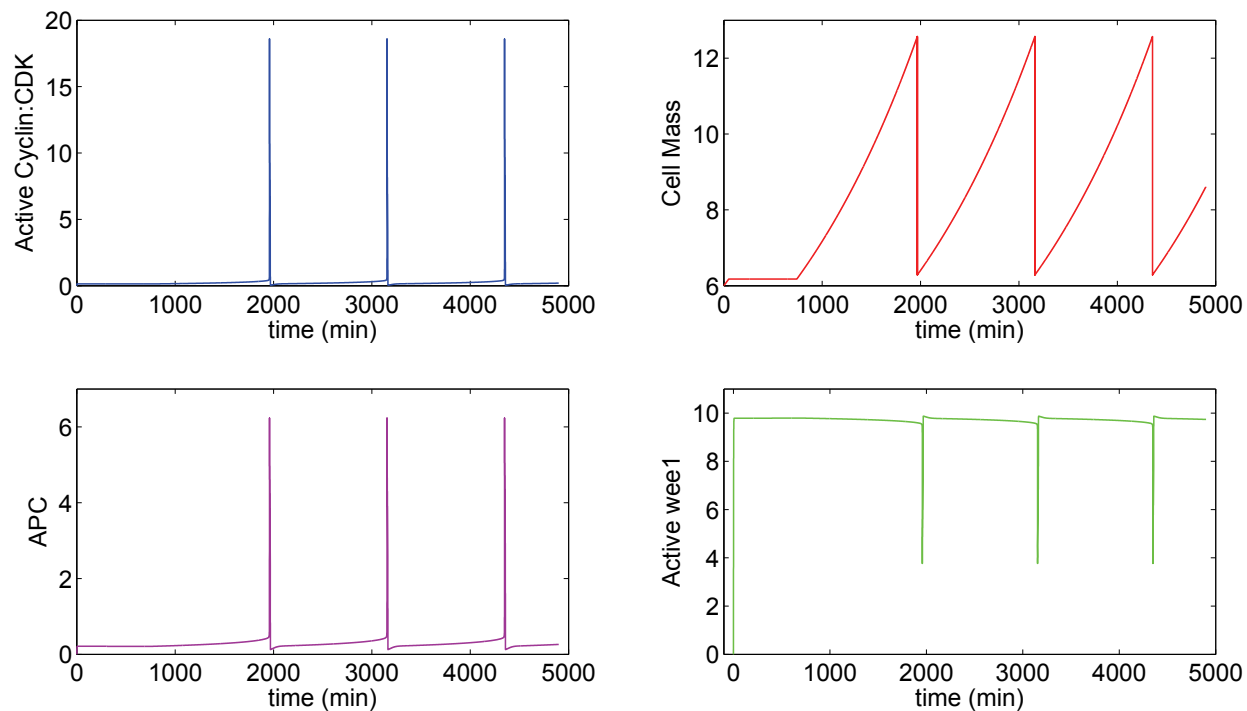
Figure 7: $G_1/S \div G_2/M$ transition species and cell mass evolution for growth halted at $t = 50 min$: (counter-clockwise) active cyclin-CDK complex and APC are only apparently in-phase due to pictorial rendering. Computational analysis shows constant lead angle of 7.8×10^{-7} Hz between these two species. Conversely, wee1 is exactly in phase modulation with active cyclin-CDK (being the pulsing frequency of 4.7×10^{-2} Hz). Cell growth arrest persists until DNA damage is totally repaired; this implies a time-shift in the species dynamics directly linked to the period of cell cycle arrest. Once the cell mitotic process occurs, the $G_1/S \div G_2/M$ transition species claw back their pulsing frequency (see Qu et al. 2003a-b).
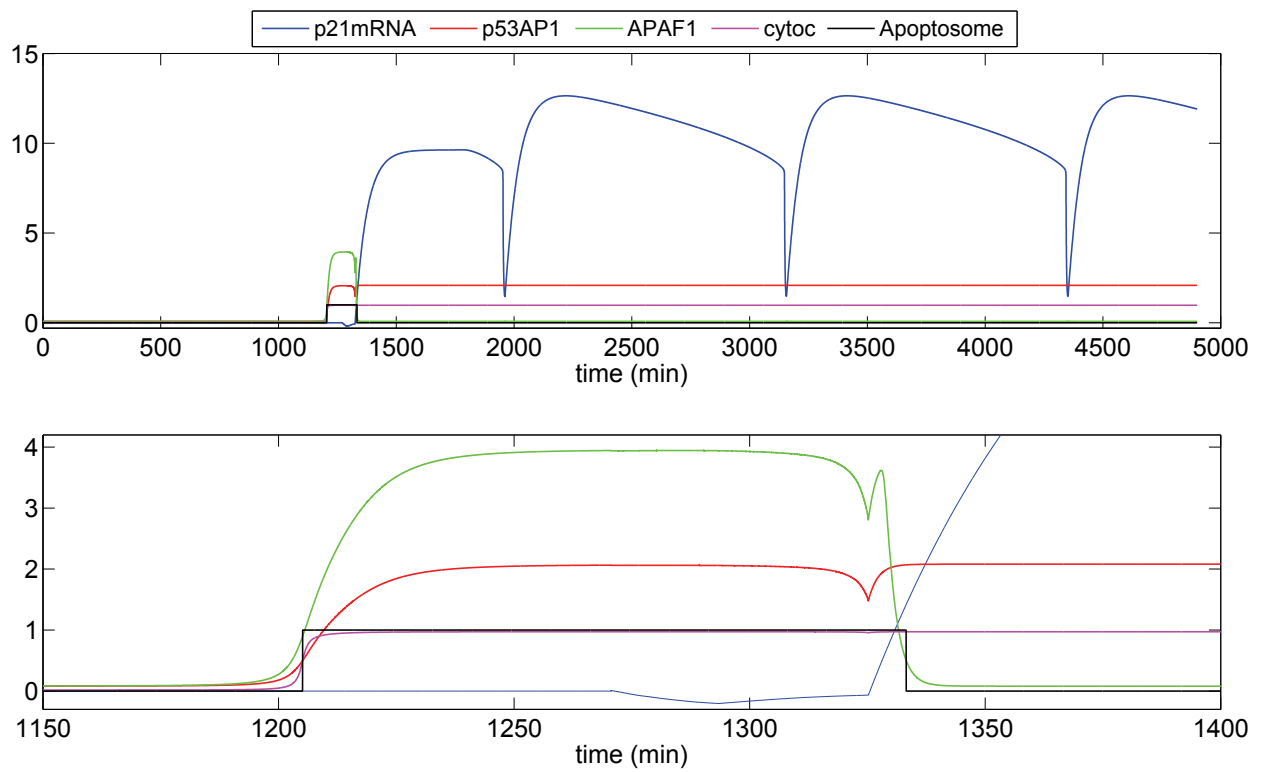
Figure 8: Output response of apoptotic species network as a consequence of DNA damage at $t = 1100min$: pictorially, the digital species pathways simulate growth arrest until DNA damage is completely repaired (see cell mass panel of Fig. 9). Close-up of apoptosis time window is shown within the timespan $1150 \div 1400min$ (below).
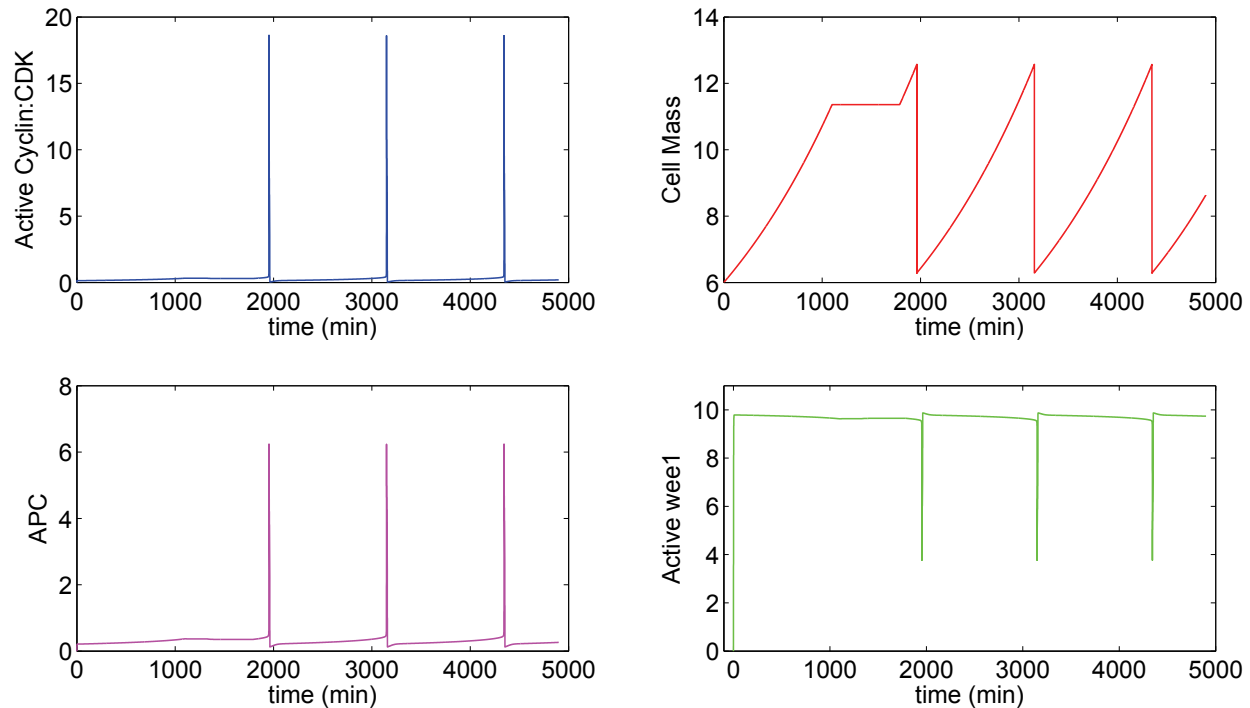
Figure 9: $G_1/S \div G_2/M$ transition species and cell mass evolution for growth halted at $t = 1100min$: all the oscillating parameters, in terms of interpulse and time delay, remain the same as those of Fig. 7 (see Qu et al. 2003a-b).

2.6 p21mRNA "tracking" signaling and apoptosis network

Normally, if DNA damage affects genome integrity during the physiological cell cycle, a molecular emergence system is immediately activated. Once the bleeps process a DNA damage progression, the cell cycle is halted and the p53/Mdm2 double-feedback network pulses.

Essentially, the digital behavior of a p53/Mdm2 feedback loop consists of zero, one, two or more pulses as a function of DNA damage (see Ma et al. (2005), Geva-Zatorsky et al. (2006), Shangary and Wang (2008), Ciliberto et al. (2005), Zhang et al. (2007), Bates et al. (1998), Bar Or et al. (2000), Bell et al. (2002), Lahav et al. (2004), Loewer and Lahav (2006), Ventura et al. (2007), Batchelor et al. (2008), Vassilev et al. (2004), Meek (2004), Vousden et al. (2002), Haupr et al. (2003), Ardito Marretta and Marino (2007), Ardito Marretta et al. (2008), Fiscella et al. (1997), Oda et al. (2000)). Therefore, at each pulse, DNA damage decreases (see Ardito Mar-

retta (2009a-b), Ciliberto et al. (2005), Zhang et al. (2007)). Based on previous studies (Ardito Marretta et al. (2009a), Ciliberto et al. (2005), Zhang et al. (2007)), a key role is also played by p21mRNA and its dynamics. If irreversible DNA damage is present, p21mRNA synthesis remains almost quiescent at the beginning of the apoptotic time window but triggers suddenly with concurrent and specific pathways of apoptotic target genes having as a consequence the closure of the apoptotic time window and allowing the cell to avoid its fate.

This peculiar and malicious mechanism of p21mRNA was previously studied by the first author (Ardito Marretta (2009a)) to identify its interaction with apoptosis genes. In that previous digital approach, the results are in experimental agreement with those of Viale et al. (2009) even though only the p53/Mdm2/p21 and p53AIP1/APAF1/cytoc were considered. In that case, p53-independent p21mRNA overexpression showed unforeseen dynamics when related to the apoptosis gene pathways. When different signals

of p21mRNA were triggered, the response of the p53/Mdm2 network radically changed into an impulse train of prolonged undamped oscillations whose amplitude and frequency were one order higher than in the case in which the DNA was quickly repaired (see Ardito Marretta, (2009a-b)) and in agreement with the observations of Ghosh and Bose (2006).

Looking (clockwise) at the panels of Figure 10, one can deduce the p21mRNA signal dependence of apoptosis and demonstrate a "digital-sequenced tracking radome" property of p21mRNA for instantly identifying the wavelengths and frequencies of the apoptotic species and intercepting their gradient inversions. To elucidate and confirm this (unforeseen) general mechanism, we manipulate different signal pathways of p21mRNA over different triggering timespans.

At first, let p21mRNA be represented by a negative linear-ramp signal in an aberrant cancer cell. Digital processes are performed over two timespans, 114.4÷144.85min, in phase with "natural" apoptotic time window, and 200÷1200min, respectively (see Ardito Marretta, 2009a-b).

For the first timespan, the results sketched in Fig. 10 (see "*p21 negative in Apoptosis*" panel) show p21mRNA upregulation almost vanishing and the remaining apoptotic species release their brakes and freely pulse toward a choral tuning at the same inflexion point at the same time location. The consequent apoptosis phase has no need of a second pulse to become permanently active.

The "tracking" properties of p21mRNA are confirmed even though it is again conceived as a negative linear-ramp signal all over a time-span of 200÷1200min, i.e., past the natural apoptotic phase in the presence of irreparable DNA damage (see Fig. 10, "*p21 negative post Apoptosis*" panel). In fact, p21mRNA overexpression immediately triggers to intersect the inflexion point of APAF1 time rate.

This successfully occurs but two parameters come into play and change p21mRNA pathway: 1) inversion of the p21mRNA upregulation time rate and, 2) the second pulse of APAF1. p21mRNA,

as a processor, exploiting to the utmost its direct "tracking memory" access, tries to follow this second pulse of APAF1 at its inflexion point for intersection. This is allowed for the second time but the third chance is denied because APAF1 reaches a steady-stable condition. According to this pulsating species dynamics, the apoptosis phase again shows two pulses and remains unchanged but with a frequency slightly lower (1.74×10^{-4}) than the natural frequency of the (unstable) apoptotic phase of a cancer cell with irreparable DNA damage.

The results sketched in the last two panels of Figure 10 confirm the above assertions. Now, the simulations are performed using a different p21mRNA pathway (mono-cycle square-wave signal) over the same timespans (114.4÷144.85min (apoptotic time window) and 200÷1200min, respectively). The only difference is that the p21mRNA upregulation tries to intersect the APAF1 inflexion point during its first pulse (having an extremely high frequency equal to 3.61×10^{-4}) but the available remaining time window is too short for a second attempt. The apoptosis phases for both the considered timespans remain active with unchanged double-cycle pathways and natural frequencies. The simulation output for 200÷1200min (past apoptotic natural time window) is qualitatively the same as those relative to 114.4÷144.85min. To widely extend, check and clarify not only the peculiar p21mRNA properties but also its interaction with the overall cell cycle dynamics and parameters, we improved the cell master digital simulator design by interlinking p21mRNA/cyclin-CDK complex and CDK/CDC25/wee1/SKP2/APC/CKI networks to the apoptotic mechanism. In other words, the goal of the present paper is to find a method to select cell checkpoints, sizers, timers and specific target gene dynamics both for influencing mitotic process and avoiding cancer proliferation as much as for leading the cancer cell(s) to re-enter a steady stable apoptosis phase (see details in the next section).
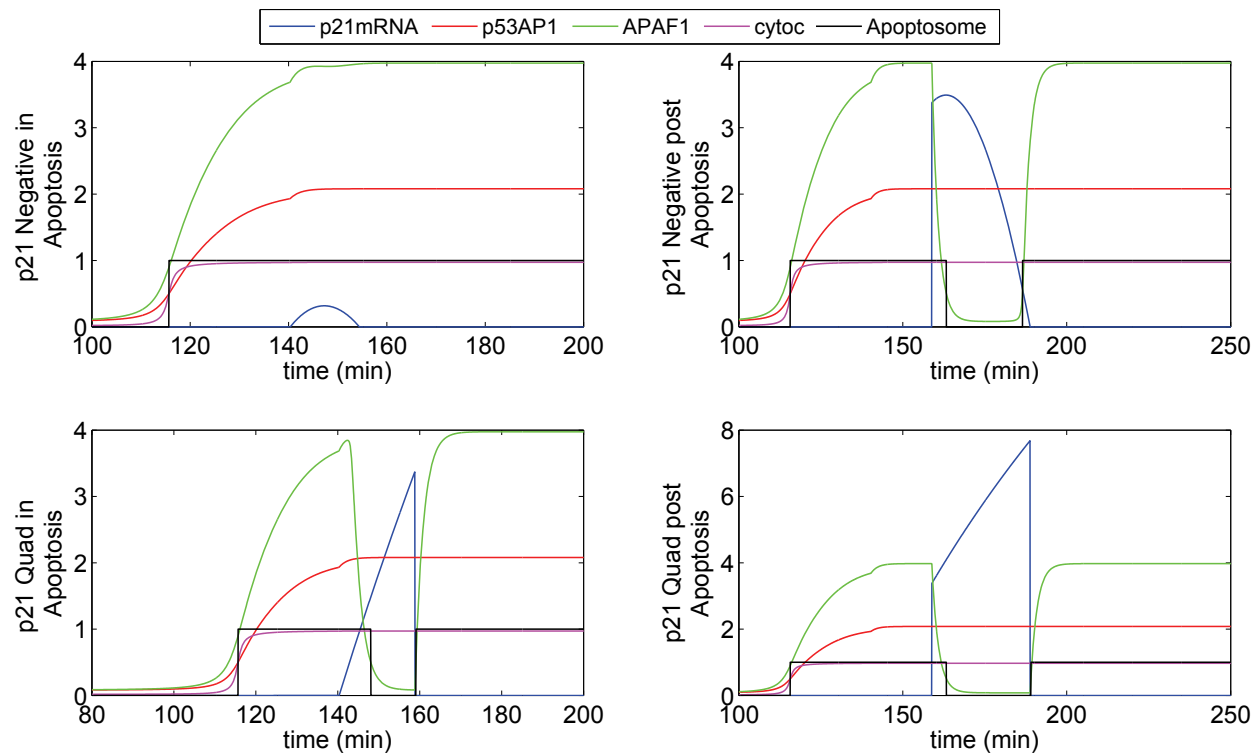
Figure 10: Stand-alone apoptotic response control system (clockwise): above-left) output response of apoptotic target gene network having as input a p21mRNA negative linear-ramp signal in phase with apoptotic natural timespan of 114.4÷144.85min (see Ardito Marretta 2009a-b). Gene dynamics shows relative saturation levels and has a choral inflexion point; then, the apoptosis phase starts. p21mRNA overexpression is almost vanishing and its "tracking" properties are lost. Apoptosis triggers in-phase with choral inflexion points; above-right) output response of apoptotic target gene network having as input a p21mRNA negative linear-ramp signal applied at the end of apoptotic natural timespan of 114.4÷144.85min. p21mRNA overexpression oscillates to track the inflexion points of APAF1 double pulses. Apoptosis is in phase-delay with p21mRNA starting overexpression and shows two distinct pulses; below-right) output response of apoptotic target genes network having as input a p21mRNA impulse square-wave signal in phase with apoptotic time window over a timespan of 124.4÷158.85min. The input signal affects the pathway of p21mRNA response, but the overall behavior of the apoptotic species remains similar to the previous one; below-left) output response of apoptotic target genes network having as input a p21mRNA impulse square-wave signal at the end of the apoptotic natural timespan of 114.4÷144.85min. Once more, the input signal affects the pathway of p21mRNA response, but the overall behavior of the apoptotic species remains similar to the previous one.

2.7 Unarrested cell cycle depending on DNA damage target genes response

In order to determine whether and how aberrant cell response to oncosuppressor signaling affects its cycle, we conducted a series of simulations in which cell cycle arrest was by-passed during DNA damage repair. Cell digital multi-layers stimulate genomic damage by the onset of two square-wave radiation signals exerted for 10min and triggered in the G_1 phase (Simulation Starting Time, (*SST*), t=0min) and in the G_2/M transition phase (*SST*, t=1100min), respectively. As regards the p21mRNA "tracking mode" signals, we used those displayed in Fig. 10 for the controlled cell digital neworks.

Apoptotic target gene interactions as a response to the DNA damage impulse at t=0min (see Fig. 11) confirm and reveal once more p21mRNA overexpression as a consequence of p53AIP1, APAF1 and cytoc instability of their pathways located at 235.6÷235.8min. After a transient of 2.27min, in which APAF1 restarts to increase its concentration, natural p21mRNA "tracking mode" overexpression signaling (solid line in Fig. 11) leads APAF1 to decrease up to its lowest concentration at t=257.43min. Both overexpression of p21mRNA and degradation of APAF1 occur with high speed rates (gradients). Post-processing analysis of Fig. 11 also reveals the closure of the apoptotic time window once APAF1 begins to fall.

This peculiar connection between Apoptosome and APAF1 was also observed in the earlier simulations (see Figs 6, 8 and 10) revealing a key role played in cell fate by APAF1 concentration. On the other hand, in the p21mRNA controlled "tracking" signaling simulation (dashed line in Fig. 11), all the apoptotic species pathway behaviors coherently remain the same as those obtained with natural p21mRNA signaling over 0<t<237.92min. Meanwhile, once the pathway instabilities of p53AIP1, APAF1 and cytoc vanish for t>237.92min, APAF1 and Apoptosome concentrations remain overexpressed and steady stable. During the natural p21mRNA signaling, at t=237.92min, the APAF1 time rate becomes negative and its concentration drops to zero; in-

stead, for the digital controlled p21mRNA signaling, this does not occur.

High concentration of APAF1 and steady stable apoptosis confirm the prominence of APAF1 as a co-actor in executing cell fate; moreover, for 0<t<237.92min, natural and controlled apoptotic target genes pathways are almost superimposable. Different responses for cell fate are activated when *SST* exceeds this limit (t>237.92min) depending on p21mRNA oscillations, i.e., if cell digital machinery acts on p21mRNA interpulses, execution of programmed cell death is successfully obtained; if not, cell fate is avoided. As regards cell cycle growth factors, the natural p21mRNA oscillations and DNA damage repair actions affect timers (as in the arrested cell cycle simulation) and sizers (see Fig. 12). In this case, cell division undergoes a time delay of t=27.1min causing the cell to yeast further. This time delay arises from the (negative) feedback loop between active Cyclin-CDK and p21mRNA. During DNA damage repair, the p53/Mdm2 pulsing response upregulates p21mRNA which, in cascade, reacts to delay overexpression of cell cycle species (active Cyclin-CDK and APC, particularly) the global effect being the transfer of timer delay and sizer variation from parent cell to daughters. At this stage, closure of the apoptotic time window (see Fig. 11) allows the aberrant cell to enter the mitotic phase and damage propagation. If p21mRNA "tracking" signaling is controlled, the apoptotic time window matches the steady stable condition and cell fate is executed at t=615.66min, before the cell enters the mitotic phase and tumorigenesis is removed.

When the radiation signal triggers at t=1100min, DNA damage occurs just before cell division. In this case, the apoptotic network is activated and its target gene overexpression is imposed on the mother cell at t=1171.56min which continues to grow until *M* checkpoint (mitosis). At this stage, cell division has no influence on the apoptotic target genes (see Fig. 13). Sequentially, p21mRNA overexpression persists again to coincide with instabilities of p53AIP1, APAF1 and cytoc pathways at 1325.17÷1325.22min but a remarkable difference emerges, i.e., p21mRNA

overexpression occurs in daughter cells. This implies that the digital multi-layer scheme can assign controlled molecule kinase and biochemical factor evolutions for meeting cell fate decision at an exact instant (t=1705.12min), past the mitotic process time (t=1227.1min), in the daughter cells. For this second set of simulations, apoptotic gene pathways are quite similar to those displayed in Figures 8 and 11 but they show a shift of t=1100min. Once again, if DNA damage affects G_2/M, Apoptosome steady stable "switch on" mainly depends on the APAF1 pathway response (see green lines in Fig. 13).

Without going into further detail, the genomic repair action is irrelevant on timers and sizers for the first mitotic step (see Fig. 14), in fact for t<1227.1min, p21mRNA overexpression has not yet occurred and active cyclin-CDK/APC network does not become aware of DNA damage and oscillates (for the first division) with its own interpulse frequency. Conversely, p21mRNA overexpression triggering in daughters affects (in negative feedback loop) the active cyclin-CDK/APC network and assigns the same mitotic delay and sizer variation as the previous simulation when DNA damage was considered at t=0min (t=27.1min and Δs=0.35, respectively). Looking at p21mRNA controlled "tracking" signaling (dashed line in Fig. 14), although DNA damage is present in the mother cell, execution of programmed cell death is applied in daughters at t=1705.12min.

2.8 Unarrested cell cycle depending on DNA damage target genes response for wee1 mutated specie

Without loss of generality, we considered the wee1 synthesis rate (k_{10}) reduced one order (k_{10}=1) giving the mutant form, *wee1(-10)*. To evaluate the mutant cell response to genomic damage, we again ignored cell cycle arrest during damage repair for the same two square-wave radiation signals previously employed. For ionizing irradiation at t=0min, *wee1(-10)* does not affect the apoptotic target gene response for both controlled and uncontrolled cell digital biochemical mechanisms; pictorial depications of APAF1,

p53AIP1, cytoc and Apoptosome (see Fig. 15) are the same as those obtained for the simulations described in the previous section (see Figs 11 and 13). To evaluate the global effects on cell cycle, we compare p21mRNA pulsing frequency as obtained by Qu et al. (2003), over the timespan 0<t<2268.35min, to its proper oscillations. Mutated wee1 promotes initial unstable behavior of the cell division control species (two close concentration peaks of active cyclin-CDK and APC) and immediate cell division at t=75.04min triggers (see Fig. 16); as a consequence, at the end of its cycle, the bud mass is half a "normal" cell size. Thus, we can digitally assign a key role to mutant/wild-type wee1 for inducing cell sizer and checkpoint mutations in agreement with *in vitro* evidence experimentally confirmed by Dealy et al. (1999), Wang et al., (1999) and Qu et al., (2003a). In our model, at t=235.7min, a second instability of active cyclin-CDK and APC is connected with both p21mRNA and apoptotic gene overexpressions. After a natural inertia, t=236.26min, this second pathway instability of active cyclin-CDK and APC gives the "green light" to another mitosis. Almost surprisingly, despite this second unexpected division, the cell sizer will not be further affected because daughter cells will grow over a timespan 65.5% greater than a normal sizer; then, the cell resumes its interpulse frequency (timer) and "mutant" size, the sizer being about one half a normal cell size. If p21mRNA "tracking" signaling is controlled, apoptosis is independent of the two aberrant mitotic processes (one at t=75.04min and one after p21mRNA overexpression at t=235.7min) and cell death is successfully executed at t=615.65min.

When the ionizing irradiation signal starts at t=1100min, apoptotic network responses are the same (and only shifted) as those obtained for t=0min (see Fig. 17). Cell growth factor dynamics, in terms of sizer and timer variations, persist in such a mutant wee1 presence and are qualitatively the same as those displayed in Fig. 16, (see Fig. 18). Natural p21mRNA "tracking" signal triggering and the extent of the genomic damage (if not completely repaired) push the overall cell system towards tumorigenesis; meanwhile, if
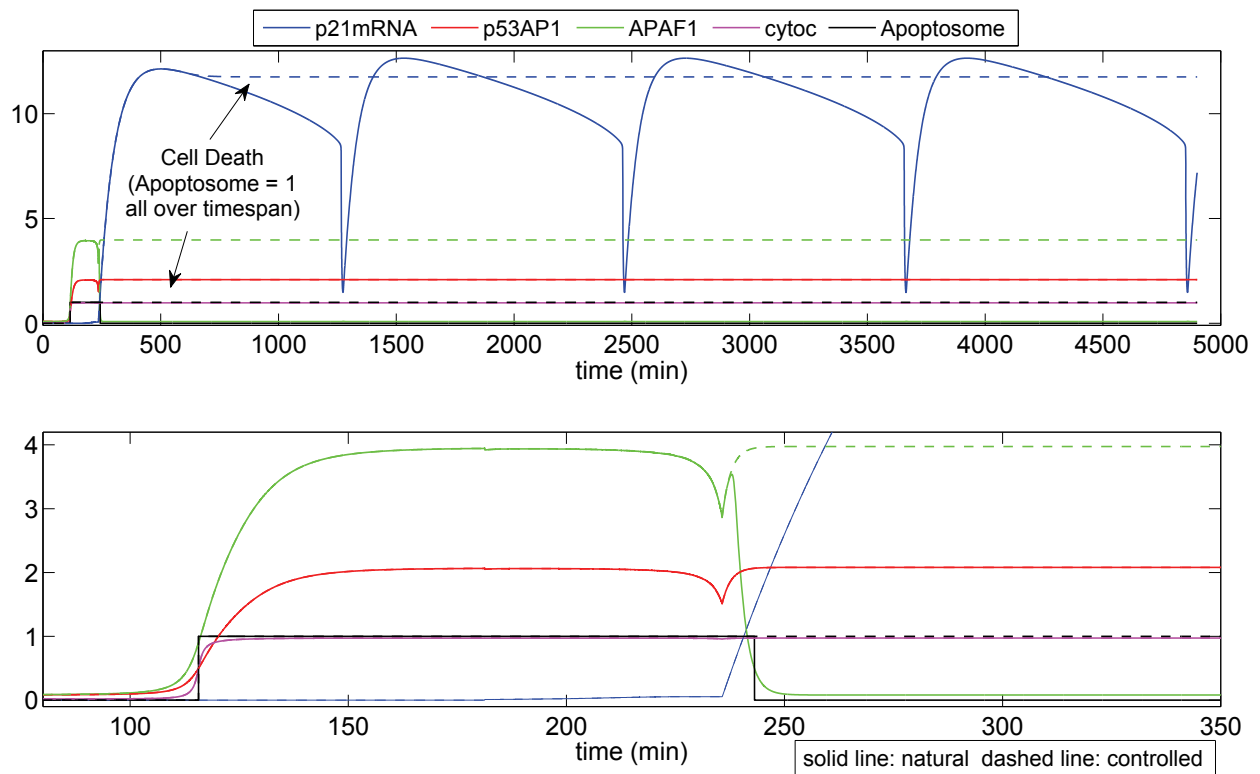
Figure 11: Output response of apoptotic species network as a consequence of a DNA damage at $t = 0min$: pictorially, the species digital pathways simulate continuous cell growth regardless of DNA damage level (see cell mass panel of Fig. 12) and in spite of the observed cell cycle arrest response to DNA damage signal. Both the natural and the controlled cell behaviors are taken into account. In the natural behavior (solid line), apoptosis only occurs for a short time window and the cell undergoes tumorigenesis. Conversely, in the controlled behavior (dashed line), apoptosis matches a steady stable active phase all over the simulation timespan and tumorigenesis is avoided. These data unravel the p21mRNA input signal-independent mechanistic contribution of apoptotic species to cell fate.
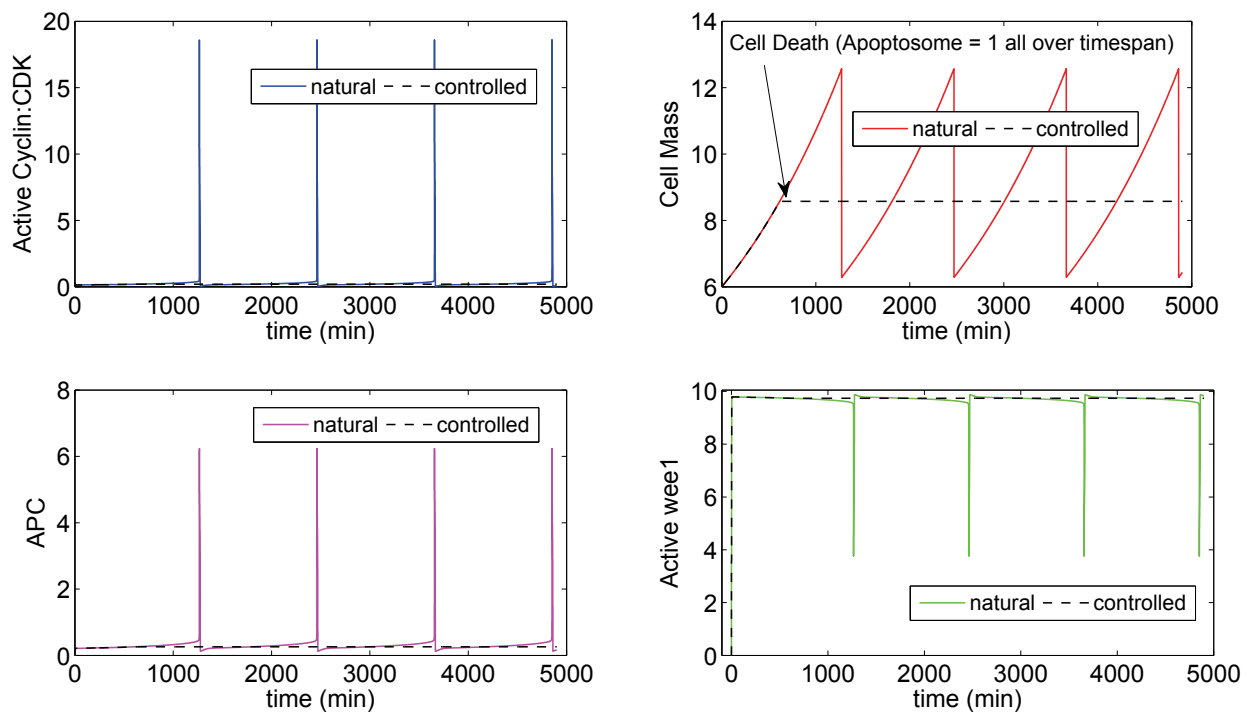
Figure 12: $G_1/S \div G_2/M$ transition species and cell mass evolution (growth not halted and DNA damage starting at $t = 0min$): for natural (uncontrolled) species behavior, the oscillating parameters, in terms of interpulse, remain the same as those of Fig.7. On the other hand, results display a time delay of $692.2min$ which depends on the time-dependent DNA damage signal and growth arrest. Compared to natural cell cycle dynamics, unarrested growth, in presence of a DNA damage, induces a constant lead angle of 3.1×10^{-5}Hz for each target species. In the controlled system, cell death triggers earlier than gene dynamic oscillations.
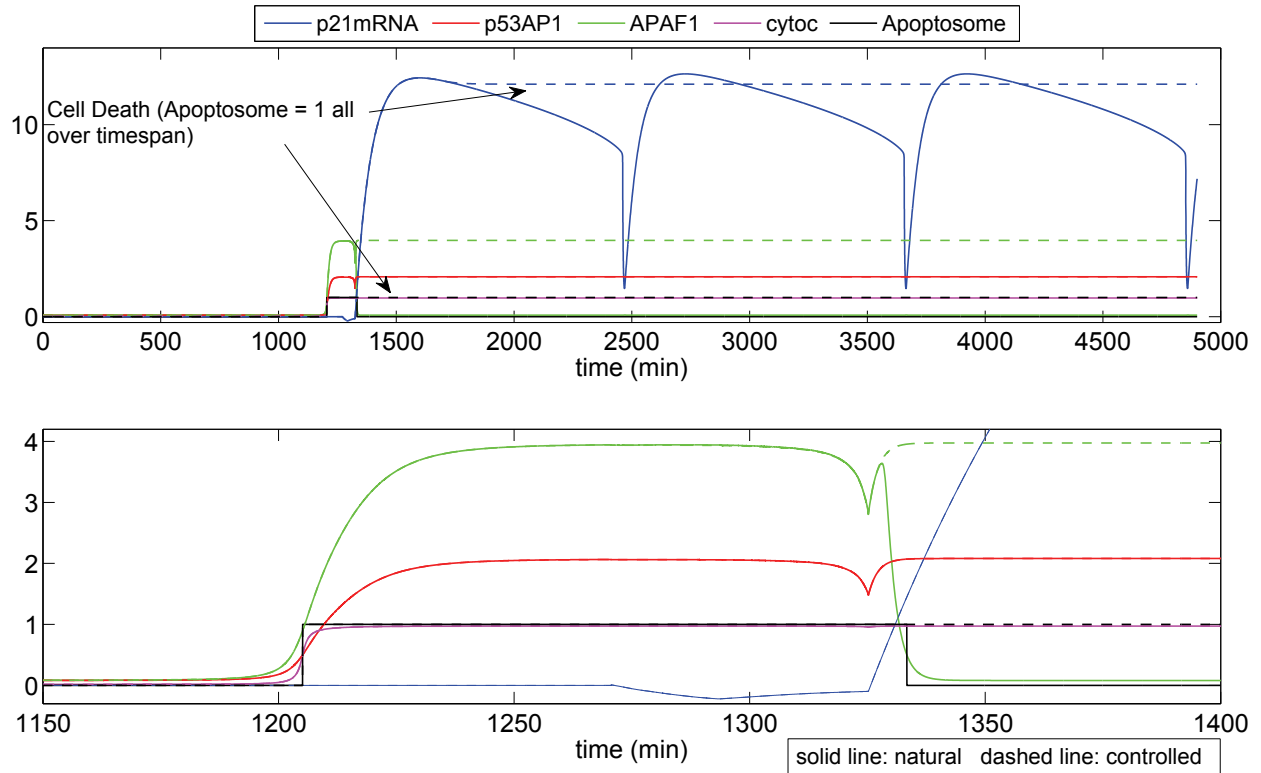
Figure 13: Output response of apoptotic species network as a consequence of DNA damage at $t = 1100min$: digital species pathways simulate continuous cell growth regardless of DNA damage in G_2/M transition phase and Apoptosome matches unit value at $t = 1205.12min$ (above). The close-up view (below) is useful in showing that the apoptotic species network is not affected by cellular mitotic progress. As a consequence, even though apoptotic target genes properly trigger within the mother cell, the cell fate execution involves the daughters. Reasonably, also G_2/M transition is not altered by the p21mRNA input signal.
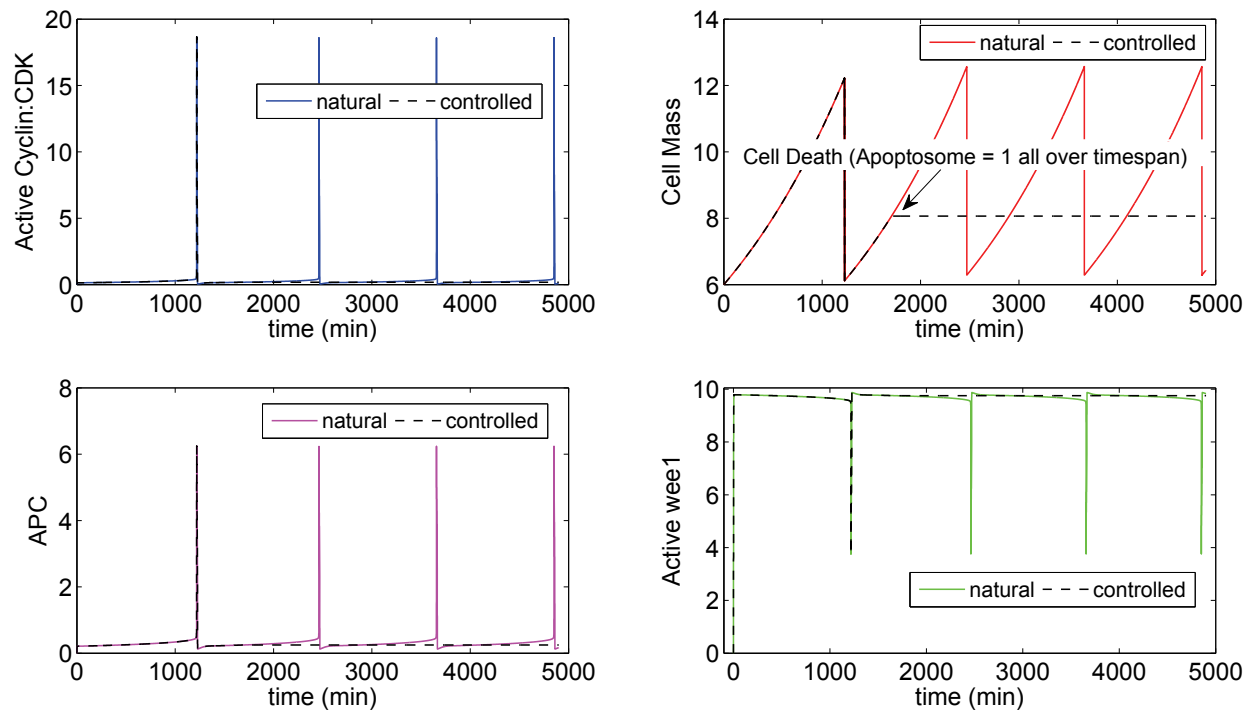
Figure 14: $G_1/S \div G_2/M$ transition species and cell mass evolution (growth not halted and DNA damage starting at $t = 1100min$): (counterclockwise) for natural (uncontrolled) species behavior, the oscillating parameters, in terms of interpulse, remain the same as those of Fig. 7 except for the second peak being the first interpulse equal to 8.1×10^{-4}Hz while the other peaks re-enter within the same bandwidth of Fig. 7. On the other hand, the results display a time delay of $740.06min$ which depends on the time-dependent DNA damage signal and growth arrest. Compared to natural cell cycle dynamics, unarrested growth, in the presence of DNA damage, induces a constant lead angle of 3.1×10^{-5}Hz for each target species after the second peak (mitotic process accomplished). In the controlled system, cell death triggers after the first mitotic process.

p21mRNA upregulation signaling is governed by an optimum control law (dashed line in Fig. 18) proliferation is halted whatever the cell divisions. Similarly, when the ionizing irradiation signal is emitted at t=1100min and the third mitotic process is overcome, programmed cell death is executed at t=1705.15min.

3 Discussion

To check the reliability of the employed multi-nested digital platform vs. *in vitro* evidence, we also take into account the analysis of the effects of PML-RAR on p21 in p53 for leukaemia stem cells showed by Viale et al. (2009) in which p21 upregulation by PML-RAR is p53-independent. Once the digital platform was tuned to replicate this network signaling, we obtained a frequency (for two pulses) of 7.4×10^{-5} vs. 7.092×10^{-5} (Viale et al. (2009)) and a relative error of 4% (data not shown here, (see Ardito Marretta (2009a-b), Viale et al. (2009)). In agreement with but differently from Viale et al. (2009), we deduce and confirm that p21mRNA upregulation is p53-independent over the initial frame of the global timespan. The discrepancy between our results and those of these authors is superficial not only computationally speaking. In fact, the overexpression of p21mRNA digitally triggers within a very small interval and its intensity (and gradient), more similar to a saturation signal, is quite different from those of the other gene expressions. This behavior, typically digital, implies two effects: first, p21mRNA upregulation becomes almost "invisible" when one has to evaluate its effects in back-reactions and experimental tools might fail in detecting it unless they are provided with suitable digital "plug-ins"; secondly, if one admits as negligible the p53-dependence of p21mRNA overexpression, this could become supercritical for the apoptotic network. Roughly speaking, the involvement of p21mRNA in apoptosis avoidance is unveiled taking into account APAF1 as a marker.

In this way, peculiar features of the proposed model are underlined if one considers that these digital cell layers are now capable of detecting and controlling molecule signaling pathways during and (mainly) after the division process if cell growth is not arrested (see "*Cell Mass*" panels in Figs 16 and 18). In this case, the cell digital control platform is independent of DNA damage triggering and switches itself from single cell to multi-cellular configuration, i.e., it starts to sequence and control cell divisions and acts successively on the cell cycle dynamics parameters of both mother and daughters. In other words, if a damaged genome is detected and p53/Mdm2 defects, the controlled cell defence resources alarm checkpoints, timers and sizers to avoid proliferation and/or execute programmed cell death. This set of by-products is digitally highlighted by the peculiar and different double-pulsing outfits of p21mRNA (chorally with active-CDK complex, cell mass, wee1 and APC) depending both on apoptotic gene instabilities and cell cycle time windows.

As regards the apoptotic species network only, it switches on the alert at an exact time location, i.e., when the target gene gradients—even though still growing—start to invert their time rates. This universal convergence criterion leads to the gene gradients for decrypting the apoptosis code.

The proposed cell digital simulator model demonstrates how the whole cell apoptosis network rigorously falls into line with this principle and suggests the mechanism for apoptosis stimulation and stabilization.

The relevance of the problem of p21mRNA upregulation influence on apoptotic target gene networks may be questioned on the grounds that it was hitherto unknown how the p21mRNA instantaneous time rate in a cancer cell affects the cell mechanism switching properties to activate apoptosis and/or downstream target species.

In the proposed method of attack, details of the p21 expressions are estimated from biological principles and not only from the dynamics of the p21mRNA species; at the same time, as soon as the apoptotic effects are deduced, we preclude the discussion of this phenomenon where there is a significant back-reaction of the p21mRNA itself.

We also submit to the biological research audience the proposal that a cellular system of target genes should be devised for experimentally
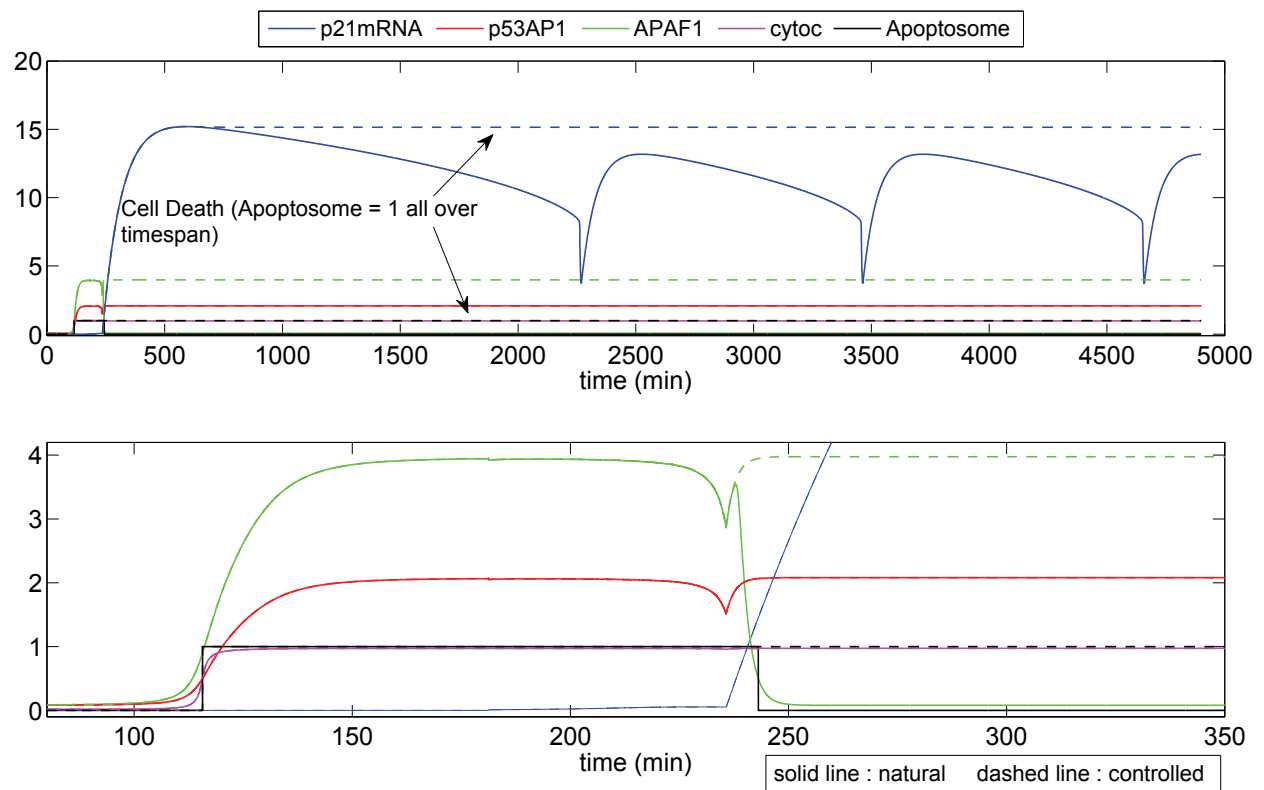
Figure 15: Output response of apoptotic species network as a consequence of DNA damage at $t = 0min$ for mutant wee1 ($k_{10} = 1$): the displayed results confirm those concerning tumorigenesis and/or apoptosis triggering both in natural and controlled cell cycle behaviors. Again, for a mutant cell, these data unravel the p21mRNA input signal-independent mechanistic contribution of apoptotic species to cell fate.
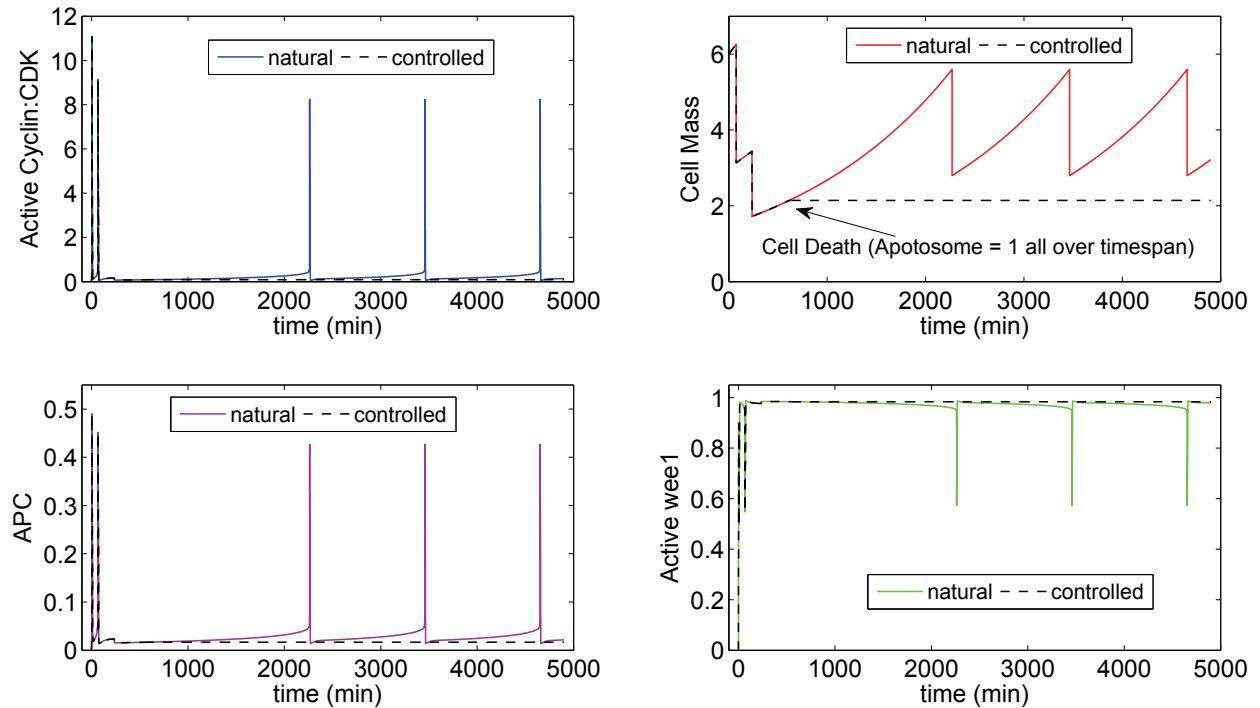
Figure 16: $G_1/S \div G_2/M$ transition species and cell mass evolution (growth not halted and DNA damage starting at $t = 0min$) for mutant wee1 ($k_{10} = 1$): (counterclockwise) for natural (uncontrolled) species dynamics, the oscillating parameters show unstable first interpulse within the cell cycle timespan. Pulsing frequency achieves a stable value at $t > 2000min$. Compared to natural cell dynamics, mutant species initiate different cell cycle events in terms of sizers and timers. Results fit quite well the published data of Dealy et al. (1999), Wang et al. (1999) and Qu et al. (2003a-b); for $t > 2000min$, cell birth process occurs with the same interpulse shown in Fig.7 but at a smaller size. In the controlled system, cell death triggers once the initial unstable interpulse vanishes.
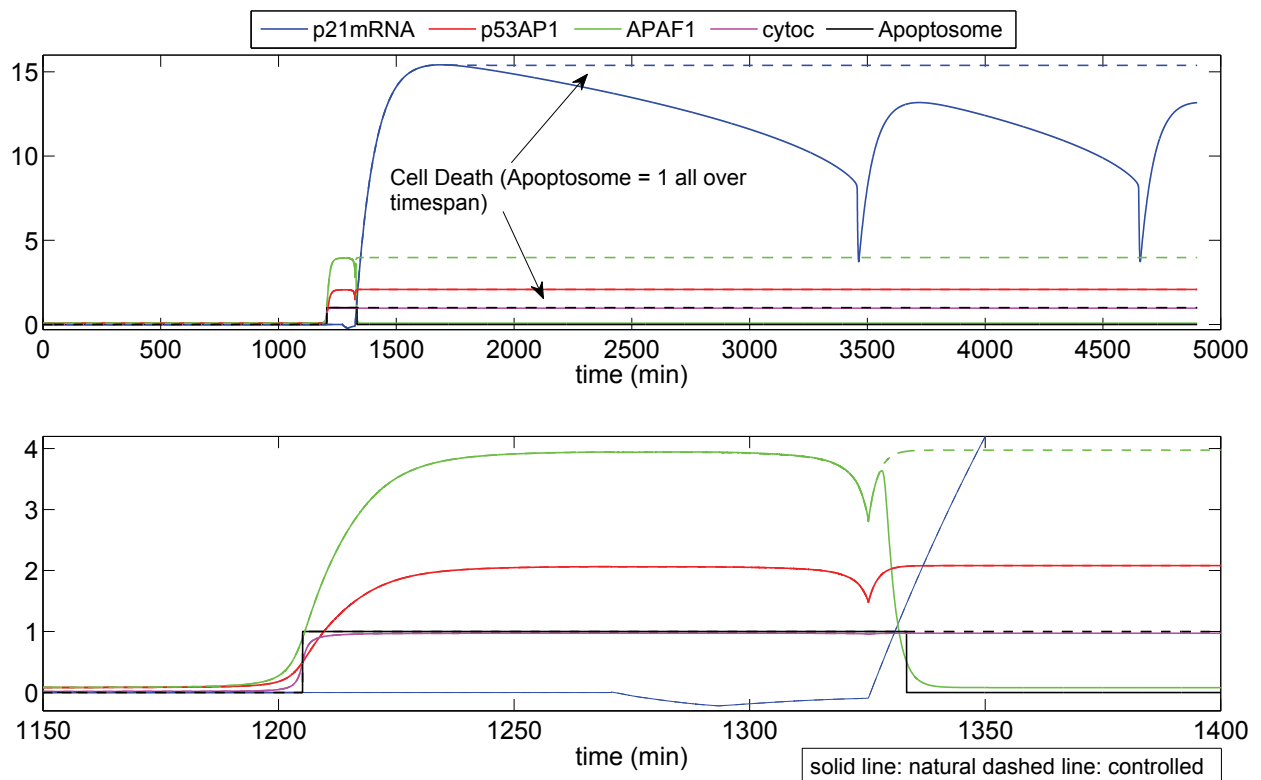
Figure 17: Output response of apoptotic species network as a consequence of DNA damage at $t = 1100min$ for mutant wee1 ($k_{10} = 1$): the displayed results confirm those concerning tumorigenesis and/or apoptosis triggering both in natural and controlled cell cycle behavior. Again, for a mutant cell, these data unravel the p21mRNA input signal-independent mechanistic contribution of apoptotic species to cell fate.
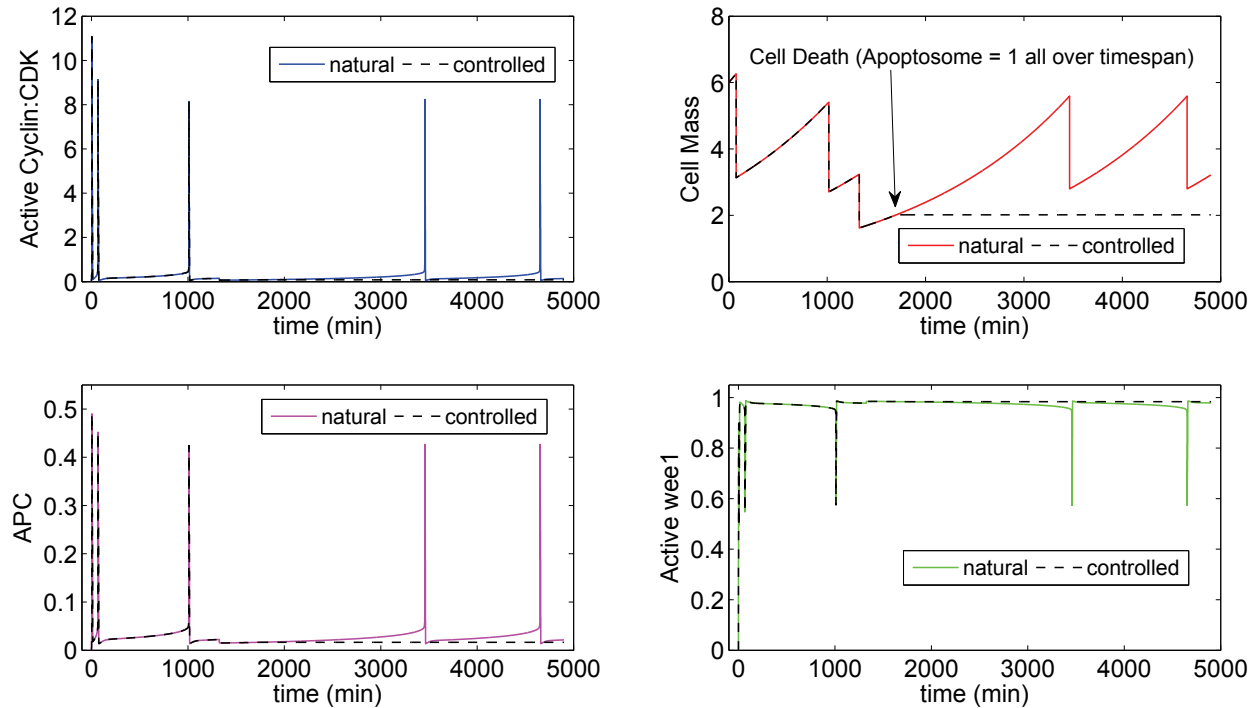
Figure 18: $G_1/S \div G_2/M$ transition species and cell mass evolution (growth not halted and DNA damage starting at $t = 1100min$) for mutant wee1 ($k_{10} = 1$): (counterclockwise) for natural (uncontrolled) species dynamics, the oscillating parameters show unstable first interpulse within the cell cycle timespan. Pulsing frequency achieves stable value at $t > 3500min$. Compared to natural cell dynamics, mutant species initiate different cell cycle events in terms of sizers and timers. Again, results fit quite well the data of Dealy et al. (1999), Wang et al. (1999) and Qu et al. (2003a-b); for $t > 3500min$, cell birth process occurs with the same interpulse displayed in Fig.7 but at a smaller size. In the controlled system, cell death triggers once the initial unstable interpulse vanishes.

confirming, extending and applying the proposed model for similar or different human cell diseases. It could shed light on investigation into the mechanisms underlying stabilization methods in which the presence of proteins in cytoplasmic lysates of human RKO colorectal carcinoma cells form complexes with p21mRNA (Park et al., 2003) that are actually inducible by treatment with short-wavelength or other stress agents or to characterize endogenous p21 expression and transcriptional and translational inducibility of p21 in a panel of leukaemic cell lines. For example, one of the primary spin-offs of the proposed application could lead to a study for clarifying the importance of p21WAF1/CIP1(p21) gene expression in the tumorgenicity of hepatitis B virus (HBV) and hepatitis C virus (HCV) infected human hepatocellular carcinoma (HCC) or help to address new areas of research on the controversial aspect of the pathogenesis of Duchenne muscular dystrophy (DMD) in which abnormalities in proliferation and differentiation of the dystrophin-deficient muscle are observed (Endesfelder et al. (2000)). In this pathology, cells withdrawn from the cell cycle permanently express p21. As recognized, p21, in contrast to other cell cycle proteins, does not diminish when myotubes are re-exposed to growth media and it has been statistically recognized that increased p21mRNA levels occur in dystrophin-deficient muscle tissue.

References

Reference

1. Aguda B-D (1999) A quantitative analysis of the kinetics of the G(2)DNA damage checkpointsystem. *Proc. Natl. Acad. Sci.* U.S.A. 96:11352-11357.

2. Aguda B.D, Tang Y (1999) The kinetic origins of the restriction point in the mammalian cell cycle. *Cell Prolif.* 32:321-335.

3. Ambrosi D, Preziosi L (2002) On the closure of mass balance models for tumour growth. *Math. Mod. Meth. Appl.* 12:737-754.

4. Ambrosi D, Mollica F (2002) On the mechanics of a growing tumour. *Int. J. Engng. Sci.* 40:1297-1316.

5. Ambrosi D, Mollica F (2004) The role of stress in the growth of a multicell spheroid. *J. Math. Biol.* 48:477-499.

6. Ardito Marretta R-M, Barbaraci G (2009) Digital control circuitry of cancer cell and its apoptosis. *Mol. Cell. Biomech.* 6:175-189.

7. Ardito Marretta R-M (2010) Digital control circuitry for the p53 dynamics in cancer cell and apoptosis. *Centr. Eur. J. Biol.* 5(2):197-213.

8. Ardito Marretta R-M, Marino F (2007) Wing flutter suppression enhancement using a well-suited active control model. *J. Aero. Engng.* 221: 441-453.

9. Ardito Marretta R-M., Marino F, Bianchi P, (2008) Computer active control of damping fluid of a racing superbike suspension scheme for road-safety improvement spin-off. *J. Vehicle Des.* 46:436-450.

10. Bar Or R-L, Maya R, Segel L-A, Alon U, Levine A-J, Oren M (2000) Generation of oscillations by the p53-Mdm2 feedback loop: a theorethical and experimental study. *Proc. Natl. Acad. Sci.* U.S.A. 21:11250-11255.

11. Batchelor E, Mock C-S, Bhan I, Loewer A, Lahav G (2008) Recurrent initiation: a mechanism for triggering p53 pulses in response to DNA damage. *Mol. Cell.* 30:277-289.

12. Bates S, Phillips A-C, Clark P-A, Stott F, Peters G, Ludwig R-L, Vousden K-H (1998) p14^{ARF} links the tumour suppressor RB and p53. *Nature* 395: 124-125.

13. Bell S, Klein C, Muller L, Hansen S, Buchner J (2002) p53 contains large unstructured regions in its native state. *J. Mol. Biol.* 322:917-927.

14. Borisuk M-T, Tyson J-J (1998) Bifurcation analysis of a model of mitotic control in frog eggs. *J. Theor. Biol.* 195:69-85.

15. Bose I, Ghosh B (2007) The p53-MDM2 network: from oscillations to apoptosis. *J. Biosci.* 32:991-997.

16. Breward C-J-W, Byrne H-M, Lewis C-E (2002) The role of cell-cell interaction in a two-phase model for a vascular tumour growth. *J. Math. Biol.* 45: 125-152.

17. Byrne H-M, King J-R, McElwain D-L-S, Preziosi L (2003) A two-phase model of solid tumour growth. *Appl. Math. Letters* 16:567-573.

18. Byrne H-M, Preziosi L (2004) Modeling solid tumours growth using the theory of mixtures. *Math. Med. Biol.* 20:341-366.

19. Chaplain M, Graziano L, Preziosi L (2006) Mathematical modelling of the loss of tissue compression responsiveness and its role in solid tumour development. *Math. Med. Biol.* 23:197-229.

20. Chen K-C, Csikaz-Nagy A, Gyorffy B, Val J, Novak B, Tyson J-J (2000) Kinetic analysis of a molecular model of the budding yeast cell cycle. *Mol. Biol. Cell.* 11:369-391.

21. Ciliberto A, Novak B, Tyson J-J (2005) Steady states and oscillations in the p53/Mdm2 network. *Cell Cycle* 4:488-493.

22. Dealy M-J, Nguyen K-V, Lo J, Gstaiger M, Krek W, Elson D, Arbeit J, Kipreos E-T, Johnson RS (1999) Loss of Cull1 results in early embryonic lethality and dysregulation of cyclin E. *Nat. Gen.* 23:245-248.

23. Deguchi S, Ohashi T, Sato M (2005) Intracellular stress transmission through actin stress fiber network in adherent vascular cells. *Molecular and Cell Biomechanics* 2:205-216.

24. Endesfelder S, Krahn A, Kreuzer K-A, Lass U, Schmidt C-A, Jahrmarkt C, Von Moers A, Speer A, (2000) Elevated p21mRNA level in skeletal muscle of DMD patients and mdx mice indicates either an exhausted satellite cell pool of higher p21 expression in dystrophin-deficient cells per se. *J. Mol. Med.* 78:569-574.

25. Fantes P-A (1977) Control of cell size and cycle time in *Schizosaccharomyces prombe*. *J. Cell. Sci.* 24:51-67.

26. Fiscella M, Zhang H, Fan S, Sakaguchi K, Shen S, Mercer W-E, Vande Woude G-F, O'Connor P-M, Appella E (1997) Wip 1, a novel human protein phosphatase that is induced in response to ionizing radiation in a p53-dependent manner. *Proc. Natl. Acad. Sci.* U.S.A. 94:6043-6053.

27. Fodde R, Smits R (2002) A matter of dosage. *Science* 298:761-763.

28. Fotedar R, Bendjennat M, Fotedar A (2008) Functional analysis of CDK inhibitor $p21^{(WAF1)}$. *Check. Contr. Canc.* 281:55-71.

29. Frieboes H, Zheng X, Sun C-H, Tromberg B, Gatenby, R, Cristini V (2006) An integrated computational/experimental model of tumour invasion, *Cancer Res.* 66:1597-1604.

30. Gardner T-S, Dolnik M, Collins J-J (1998) A theory for controlling cell cycle dynamics using a reversibly binding inhibitor. *Proc. Natl. Acad. Sci.* U.S.A. 95:14190-14195.

31. Geva-Zatorsky N, Rosenfeld N, Itzkovitz S, Milo R, Sigal A, Dekel E, Yarnitzky, T, Liron Y, Polak P, Lahav G, Alon U (2006) Oscillations and variability in the p53 system. *Mol. Syst. Byol.* doi: 10, 1038:1-13.

32. Goldbeter A (1991) A minimal cascade model for the mitotic oscillator involving cyclin and cdc2 kinase. *Proc. Natl. Acad. Sci.* U.S.A. 88: 9107-9111.

33. Ghosh B, Bose I (2006) Gene copy number and cell cycle arrest. *Phys. Biol.* 3:29-36.

34. Hatzimanikatis V, Lee K-H, Bailey J-E (1999) A mathematical description of regulation of the G1-S transition of the mammalian cell cycle. *Biotech. Bioeng.* 65:631-637.

35. Haupr S, Berger M, Goldberg Z, Haupr Y (2003) Apoptosis - the p53 network. *J. Cell. Sci.* 116:4077-4085.

36. Hohenstein P (2004) Tumour suppressor genes-one hit can be enough. *PLos Biol* 2:165-166.

37. Knudson A-G (1971) Mutation and cancer: statistical study of retinoblastoma. *Proc. Natl. Acad. Sci.* U.S.A. 68:820-823.

38. Lahav G, Rosenfeld N, Sigal A, Geva Zatorsky N, Levine A-J, Elowitz M-B, Alon U (2004) Dynamics of the p53-Mdm2 feedback loop in individual cells. *Nature Genetics* doi: 10.1038 - published online (www.nature.com/naturegenetics).

39. Loewer A, Lahav G (2006) Cellular conference call: external feedback affect cell-fate decision. *Cell* 24:1128-1130.

40. Ma L, Wagner J, Rice J-J, Hu W, Levine A-J, Stolovitzky G-A (2005) A plausible model for the digital response of p53 to DNA damage. *Proc. Nat. Acad. Sci.* U.S.A. 40:14266-14271.

41. Macklin P, Lowengrub J (2007) Nonlinear simulation of the effect of the microenvironment on tumour growth. *J. Theor. Biol.* 245:677-704.

42. Masui Y, Wang P (1998) Cell cycle transition in early embryonic development of *Xenopus laevis*. *Biol. Cell.* 90:537-548.

43. Meek D-W (2004) The p53 response to DNA damage. *DNA Repair* (Amst) 3: 1049-1056.

44. Mooney D (2006) Materials to regulate cell fate in vitro and in vivo. *Molecular and Cell Biomechanics* 3:169-176.

45. Montagne J, Stewart M-J, Stocker H, Hafen S-C, Kozma S-C, Thomas G (1999) *Drosophila* S6 kinase: a regulator of cell size. *Science* 285: 2126-2129.

46. Montagnoli A, Fiore F, Eytan N, Carrano A-C, Draetta G-F, Hershko A, Pagano M (1999) Ubiquitination of p27 is regulated by Cdk-dependent phosphorylation and trimeric complex formation. *Gen. Dev.* 13:1181-1189.

47. Morris, M-C, Heitz A, Mery J, Heitz F, Divita G (2000) An essential phosphorylation-site domain of human cdc25C interacts with both 14-3-3 anc cyclins. *J. Biol. Chem.* 275:28849-28857.

48. Nakayama K-I, Hatakeyama S, Nakayama K (2001) Regulation of the cell cycle at the G1-S transition by proteolysis of cyclin E and p27Kip1. *Biochem. Biophys. Res. Comm.* 282:853-860.

49. Novak B, Tyson J-J (1997) Modeling the control of DNA replication in fission yeast. *Proc. Natl. Acad. Sci.* U.S.A. 94:9147-9152.

50. Obeyesekere M-N, Knudsen E-S, Wang J-Y-J, Zimmerman S-O (1997) A mathematical model of the regulation of the G(1) phase of $Rb^{+/+}$ and $Rb^{-/-}$ mouse embryonic fibroblast and an osteosarcoma cell line. *Cell Prolif.* 30:171-194.

51. Oda K, Atakawa H, Tanada T, Matsuda K, Tanikawa C, Mori T, Nishimori H, Tanai K, Tokino T, Nakamura Y, Taya Y (2000) p53AIP1, a potential mediator of p53-dependent apoptosis, and its regulation by SER-46 phosphorilated p53. *Cell* 102:849-862.

52. Panorchan P, Thompson M-S, Davis K-J, Tseng Y, Konstantopoulos K, Wirtz D (2006) Single-molecule analysis of cadherin-mediated cell-cell adhesion. *J. Cell. Sci.* 119:66-74.

53. Park Y-N, Chae K-J, Kwon K-W, Oh B-H, Lee K-S, Lee W-J, Park C (2003) p53 and p21WAF1/CIP1 in hepatitis B virus related hepatocarcinogenesis. *Hepatogastroenter.* 50:1292-1296.

54. Reich C-N, Oren M, Levine A-J (1983) Two distinct mechanisms regulate the levels of a cellular tumor antigen, p53. *Mol. Cell. Biol.* 12: 2143-2150.

55. Shangary S, Wang S (2008) Targeting the Mdm2-p53 interaction for cancer therapy. *Clin. Cancer. Research* 17:5318-5324.

56. Song W-J (1999) Haploinsufficiency CBFA2 causes familial thrombocytopenia with propensity to develop acute myelogenous leukaemia. *Nat. Genet.* 23:166-175.

57. Sveiczer A-B, Novak B, Mitchison J-M (1999) The size control of fission yeast revisited. *J. Cell. Sci.* 109:2947-2957.

58. Sveiczer A, Novak B, Mitchison J-M (1999) Mitotic control in the absence of cdc25 mitotic inducer in fission yeast. *J. Cell Sci.* 112:1085-1092.

59. Qu Z, MacLellan W-R, Weiss N (2003) Dynamics of the cell cycle: checkpoints, sizers, and timers. *Biophysical J.* 85:3600-3611.

60. Qu Z, Weiss J-N, MacLellan W-R (2003) Regulation of the mammalian cell cycle: a model of the G1-to-S transition. *Am. J. Physiol. Cell Physiol.* 284: C349-C364.

61. Thron C-D (1997) Cell cycle controls. In: Fall, C.P., Marland, E.S., Wagner, J.M. and Tyson, J.J. (Eds.), Computational cell biology. Springer, New York, Berlin, pp. 261-284.

62. Tsourkas A, Weissleder R (2004) Illuminating the dynamics of intracellular activity with "active" molecular reporters. *Molecular and Cell Biomechanics* 1:136-146.

63. Tyson J-J, Chen K, Novak B (2001) Network dynamics and cell physiology. *Nat. Rev. Mol. Cell Biol.* 2:908-916.

64. Tyson J-J, Csicasz-Nagy A, Novak B (2002) The dynamics of cell cycle regulation. *Bioessays.* 24:1095-1109.

65. Tyson J-J, Novak B (2001) Regulation of the eukaryotic cell cycle: molecular antagonism, hysteresis, and irreversible transition. *J. Theor. Biol.* 210:249-263.

66. Vassilev L-T, Vu B-T, Graves B, Carvajal D, Podlaski F, Filipovic Z, Kong N, Kammlott U, Lukacs C, Klein C, Fotouhi N, Liu E-A (2004) In vivo activation of the p53 pathway by small-molecule antagonist of Mdm2. *Science* 303: 1889-1893.

67. Venkatachalan S, Shi Y-P, Jones S-N, Vogel H, Bradley A, Pinkel D (1998) Retention of wild-type p53 in tumours from p53 heterozygous mice: reduction of p53 dosage can promote cancer formation. *EMBO J.* 17:4657-4667.

68. Ventura A, Kirsch D-G, McLaughlin M-E, Tuveson D-A, Grimm J, Lintault L, Newman J, Reczek E-E, Weissleder R, Jacks T (2007) Restoration of p53 function leads to tumour regression in vivo. *Nature* 445:661-665.

69. Viale A, De Franco F, Orleth A, Cambiaghi V, Giuliani V, Bossi D, Ronchini C, Ronzoni S, Muratore I, Monestiroli S, Gobbi A, Alcalay M, Minacci S, Pelicci P-G (2009) Cell-cycle restriction limits DNA damage and maintains self-renewal of leukaemia stem cells. *Nature* 457:51-57.

70. Vlach J, Henneke S, Amati B (1997) Phosphorylation-dependent degradation of the cyclin-dependent kinase inhibitor p27. *EMBO J.* 19:5334-5344.

71. Vousden K-H, Lu X (2002) Live or let die. The cell's response to p53. *Nat. Rev. Cancer* 2:594-604.

72. Wang Y, Penfold S, Tang X, Hattori N, Riley P, Harper J-W, Cross J-C, Tyres M (1999) Deletion of the Cull1 gene in mice causes arrest in early embryogenesis and accumulation of cyclin E. *Curr. Biol.* 9:1191-1194.

73. Zhang T, Brazhnik P, Tyson J-J (2009) Computational analysis of dynamical responses to the intrinsic pathway of programmed cell death. *Biophysical. J.* 97:415-434.

74. Zhang T, Brazhnik P, Tyson J-J (2007) Exploring mechanisms of the DNA-damage response. *Cell Cycle* 1:85-94.

75. Zhang Y, Henson M (2001) Bifurcation analysis of countinuous biochemical reactors. *Biotechnol.* 17:647-660.

76. Zhou J, Chen J-K, Zhang Y (2007) Theoretical analysis of thermal damage in biological tissues caused by laser irradiation. *Molecular and Cell Biomechanics* 4:27-40.